

Barrow Entropy Cosmology: an observational approach with a hint of stability analysis

Genly Leon¹ Juan Magaña² A. Hernández-Almada³ Miguel A. García-Aspeitia^{4,5} Tomás Verdugo⁶ V. Motta⁷

¹ Departamento de Matemáticas, Universidad Católica del Norte, Avda. Angamos 0610, Casilla 1280 Antofagasta, Chile

² Instituto de Astrofísica & Centro de Astro-Ingeniería, Pontificia Universidad Católica de Chile,

Av. Vicuña Mackenna, 4860, Santiago, Chile

³ Facultad de Ingeniería, Universidad Autónoma de Querétaro, Centro Universitario Cerro de las Campanas, 76010, Santiago de Querétaro, México.

⁴ Unidad Académica de Física, Universidad Autónoma de Zacatecas, Calzada Solidaridad esquina con Paseo a la Bufa S/N C.P. 98060, Zacatecas, México.

⁵ Consejo Nacional de Ciencia y Tecnología,

Av. Insurgentes Sur 1582. Colonia Crédito Constructor, Del. Benito Juárez C.P. 03940, Ciudad de México, México.

⁶ Instituto de Astronomía, Observatorio Astronómico Nacional, Universidad Nacional Autónoma de México, Apartado postal 106, C.P. 22800, Ensenada, B.C., México

⁷ Instituto de Física y Astronomía, Facultad de Ciencias, Universidad de Valparaíso, Avda. Gran Bretaña 1111, Valparaíso, Chile.

E-mail: genly.leon@ucn.cl, aldebaran.99@gmail.com, ahalmada@uaq.mx, aspeitia@fisica.uaz.edu.mx, tomasv@astro.unam.mx, veronica.motta@uv.cl

Abstract. In this work, we use an observational approach and dynamical system analysis to study the cosmological model recently proposed by Saridakis (2020), which is based on the modification of the entropy-area black hole relation proposed by Barrow (2020). The Friedmann equations governing the dynamics of the Universe under this entropy modification can be calculated through the gravity-thermodynamics conjecture. We investigate two models, one considering only a matter component and the other including matter and radiation, which have new terms compared to the standard model sourcing the late cosmic acceleration. A Bayesian analysis is performed in which we use five cosmological observations (observational Hubble data, type Ia supernovae, HII galaxies, strong lensing systems, and baryon acoustic oscillations) to constrain the free parameters of both models. From a joint analysis, we obtain constraints that are consistent with the standard cosmological paradigm within 2σ confidence level. In addition, a complementary dynamical system analysis using local and global variables is developed which allows obtaining a qualitative description of the cosmology. As expected, we found that the dynamical equations have a de Sitter solution at late times.

Keywords: dark energy, observational constraints.

Contents

1	Introduction	1
2	Cosmology with Barrow Entropy	2
2.1	Model I: Matter and an effective dark energy	3
2.2	Model II: Matter, Radiation and Effective Dark Energy	5
3	Observational constraints	6
3.1	Observational Hubble Data	6
3.2	Pantheon SNIa sample	7
3.3	HII Galaxies	7
3.4	Strong lensing systems	8
3.5	Baryon Acoustic Oscillations	9
3.6	Results from Observational constraints	9
4	Dynamical system and stability analysis	10
4.1	Stability analysis of Model I	13
4.1.1	Global dynamical systems formulation	14
4.2	Stability analysis of Model II	20
4.2.1	Global dynamical systems formulation	21
5	Summary and discussion	27

1 Introduction

In the last decades, one of the puzzles in Cosmology is the source of the accelerated expansion of the Universe at late times. The first observational evidence of such expansion comes from the high redshift type Ia supernovae (SNIa) [1], confirmed by the acoustic peaks of the Cosmic Microwave Background Radiation (CMB) [2], and recently tested with large scale structure measurements [3]. The evidence point out to the existence of a dark entity whose gravitational influence should be repulsive, being known in the community with the name of dark energy (DE). The first approach, and the most successful DE candidate to explain the Universe acceleration is the cosmological constant (CC) [4], whose introduction in the dynamical equations is simple and in agreement with the different cosmological data and can be deduced mathematically from the Lovelock theorem [5]. Despite that CC is a successful model, understanding its nature eludes us. Our best theoretical models break down under the assumption that it comes from quantum vacuum fluctuations, obtaining results that are in total disagreement with our observations (see for example [6, 7]). In this vein that we have been forced to propose other alternatives to explain the Universe acceleration, which is the reason behind the expression 'dark energy'. Another path to address the cosmic acceleration problem is modifying the General Theory of Relativity (GR) by assuming the DE is caused by either some geometrical effect (see the following compilation of models [8–12]) or a fluid with strange characteristics, such as the Equation of State (EoS) taking the form $\omega < -1/3$, which is nonstandard for baryonic matter or even for dark matter (DM) (see also the models [13–15]).

An interesting alternative to tackle the problem of the cosmic acceleration, comes from the seminal ideas on black hole physics by Hawking and Bekenstein [16], and hereafter applied to the cosmological context (see for instance [17, 18]). The formalism, known as *gravity-thermodynamics* [18], consist on deriving the Einstein equations from a thermodynamic approach by using the proportionality of entropy and horizon area, and the assumption of local equilibrium conditions. In a recent study inspired by the geometrical structure of the COVID-19 virus, [19] propose that the expected black hole surface can be increased at the quantum gravitational level if it has such an intricate structure that could cut-off down to small scale (for instance the Planck length). In this context, Barrow constructs a fractal horizon surface by increasing the black hole area (A), hence modifying its entropy as $S_B \sim A^{f(\Delta)}$, being Δ a constant exponent. By using the gravity-thermodynamics approach, [20] calculated the equations governing the cosmological evolution assuming the Barrow entropy S_B . The modified Friedmann equation contains extra terms encoded as an effective dark energy, which drives the late cosmic acceleration. An interesting feature of this scenario is that, although the effective dark energy can behave as quintessence-like or phantom-like at different epochs, the Universe dynamics converges to de Sitter solution at larger times. By applying the Holographic principle, [21] calculated the equation governing the cosmological dynamics under the assumption that holographic dark energy obey the Barrow entropy, showing that it can source the cosmic accelerated expansion. Ref. [22] provide observational constraints on the Barrow holographic dark energy using SNIa and measurements of the Hubble data. Later on, [23] investigate the evolution of an interacting holographic dark energy model component under the Barrow's modified entropy. Recently, [24] showed that a non-flat Barrow interacting holographic dark energy can reproduce the thermal history of the Universe. In addition, the authors claim that an open Universe favors an phantom regime for the effective dark energy equation of state.

Our aim is to revisit the framework of the Barrow cosmological model proposed by [20] to investigate the viability of such scenario to explain the late cosmic acceleration without a dark energy fluid. We constrain this model with several cosmological data at different scales: observational Hubble data, type Ia supernovae, HII galaxies, strong lensing systems, and baryonic acoustic oscillations. We also perform a dynamical analysis of the system equations to identify and classify the critical points and their stability, considering that the Universe is composed just by dust matter and filled with matter and radiation.

The paper is organized as follow: Sec. 2 presents the theoretical framework for the Barrow background cosmology. In Section 3 we perform a Bayesian analysis to constrain the free parameters of the model using observational Hubble data, type Ia supernovae, HII galaxies, strong lensing systems and baryon acoustic oscillations. In Sec. 4 we perform the dynamical analysis and stability of the system around the critical points. Finally, we discuss and present a summary of our results in Sec.5. In what follows we use units in which $\hbar = k_B = c = 1$.

2 Cosmology with Barrow Entropy

The equations that govern the dynamics of the Universe can be obtained from the *gravity-thermodynamics* conjecture, particularly, the Friedmann equations are retrieved by applying the first law of thermodynamics ($-dE = T dS$) to the apparent horizon of a Friedmann-Lemaitre-Robertson-Walker (FLRW) universe [18]. Analogously to black holes whose temperature and entropy are related to its horizon area A , one can assume that this principle holds for the apparent cosmological horizon, r_A , i.e. it has an associated temperature T and

entropy S in the form $T = 1/2\pi r_A$ and $S = A/4G$, where G is the Newton constant. The heat flow (energy flux) δQ through the horizon is given by

$$\delta Q = -dE = A(\rho_f + p_f) H r_A dt, \quad (2.1)$$

being ρ_f and p_f the energy density and pressure of the fluid respectively, and the Hubble parameter at scale factor a is defined as $H = \dot{a}/a$. The radius of the apparent cosmological horizon r_A is defined as

$$r_A = \left(H^2 + \frac{k}{a^2} \right)^{-1/2}, \quad (2.2)$$

where k is the spatial Universe curvature.

Recently, [19] propose an interesting modification to the entropy-area black hole relation by considering that the black hole horizon surface has a fractal structure. If the surface varies proportional to the radius as $\propto r^{2+\Delta}$, it modifies its entropy as

$$S_B = \left(\frac{A}{A_0} \right)^{1+\frac{\Delta}{2}} \quad (2.3)$$

where A is the standard horizon area, A_0 is the Planck area, and Δ is an exponent in the range $0 < \Delta < 1$. This exponent quantifies quantum deformations, when $\Delta = 1$ the deformation is maximum and the Bekenstein entropy is recovered when $\Delta = 0$.

Following the gravity-thermodynamics approach and assuming the Barrow entropy S_B (Eq. 2.3), it is possible to obtain the Friedmann equations governing the cosmic dynamics (see further details in [20, 25]). We investigate the background Cosmology in two cases: when the Universe is filled just by matter (Model I) and by matter plus radiation (Model II). In the following, we introduce the Friedmann equation in both scenarios.

2.1 Model I: Matter and an effective dark energy

For a flat Universe ($k = 0$) filled by matter, the Friedmann and Raychaudhuri equations [20] are

$$H^2 = \frac{8\pi G}{3} (\rho_m + \rho_{DE}), \quad (2.4)$$

$$\dot{H} = -4\pi G (\rho_m + p_m + \rho_{DE} + p_{DE}), \quad (2.5)$$

where ρ_m denotes the energy density of matter (baryons plus dark matter) and we assume the equation of state $p_m = 0$ corresponding to dust (pressureless) matter. The energy density and pressure of this effective dark energy are written in the form

$$\rho_{DE} = \frac{3}{8\pi G} \left\{ \frac{\Lambda}{3} + H^2 \left[1 - \frac{\beta(\Delta + 2)}{2 - \Delta} H^{-\Delta} \right] \right\}, \quad (2.6)$$

$$p_{DE} = -\frac{1}{8\pi G} \left\{ \Lambda + 2\dot{H} \left[1 - \beta \left(1 + \frac{\Delta}{2} \right) H^{-\Delta} \right] + 3H^2 \left[1 - \frac{\beta(2 + \Delta)}{2 - \Delta} H^{-\Delta} \right] \right\}, \quad (2.7)$$

where $\Lambda \equiv 4CG(4\pi)^{\Delta/2}$, C is an appropriate integration constant and $\beta \equiv 4(4\pi)^{\Delta/2}G/A_0^{1+\Delta/2}$. Firstly, we keep β as a free parameter. Next, by setting $A_0 = 4G$ we have $\beta \equiv (\pi/G)^{\Delta/2}$.

Although Eqs. (2.4)-(2.5) does not has a dark energy component, we have dubbed *effective dark energy* the extra-terms introduced by the Barrow entropy.

The equation of state (EoS) for the effective dark energy reads

$$w_{DE} \equiv \frac{p_{DE}}{\rho_{DE}} = -1 - \frac{2\dot{H} \left[1 - \beta \left(1 + \frac{\Delta}{2}\right) H^{-\Delta}\right]}{\Lambda + 3H^2 \left[1 - \frac{\beta(2+\Delta)}{2-\Delta} H^{-\Delta}\right]}. \quad (2.8)$$

Combining (2.4) and (2.6), the dimensionless Friedmann equation takes the form

$$\frac{8\pi G\rho_m}{3H^2} + \frac{\Lambda}{3H^2} = \frac{\beta(\Delta + 2)H^{-\Delta}}{2 - \Delta}. \quad (2.9)$$

The standard model with cold dark matter and cosmological constant (Λ CDM) is recovered with $\Delta = 0, \beta = 1$, which implies

$$\frac{8\pi G\rho_m}{3H^2} + \frac{\Lambda}{3H^2} = 1. \quad (2.10)$$

Now, we define

$$\begin{aligned} \Omega_m &\equiv \frac{8\pi G\rho_m}{3H^2}, & \Omega_\Lambda &\equiv \frac{\Lambda}{3H^2}, \\ \Omega_{DE} &\equiv \frac{8\pi G\rho_{DE}}{3H^2} = 1 + \Omega_\Lambda - \frac{\beta(\Delta + 2)H^{-\Delta}}{2 - \Delta}. \end{aligned} \quad (2.11)$$

Then, from Eq. (2.9) it follows

$$\Omega_m + \Omega_{DE} = 1 + \underbrace{\Omega_m + \Omega_\Lambda - \frac{\beta(\Delta + 2)H^{-\Delta}}{2 - \Delta}}_{=0} = 1. \quad (2.12)$$

By considering that the matter component evolves in the traditional way $\rho_m = \rho_{m0}(z+1)^3$, the dimensionless Friedmann equation can alternatively be written as

$$E(z) \equiv \frac{H}{H_0} = \left\{ \bar{\beta} \frac{2 - \Delta}{2 + \Delta} [\Omega_{m0}(z+1)^3 + \Omega_{\Lambda0}] \right\}^{1/(2-\Delta)}, \quad (2.13)$$

where $a = (z+1)^{-1}$, z is the redshift, the subscripts 0 denote quantities at $a = 1 (z = 0)$, and we have defined the dimensionless parameter

$$\bar{\beta} \equiv \frac{H_0^\Delta}{\beta} = \frac{H_0^\Delta A_0^{1+\Delta/2}}{4(4\pi)^{\Delta/2} G} = \underbrace{H_0^\Delta (G/\pi)^{\Delta/2}}_{\text{setting } A_0=4G}, \quad (2.14)$$

where we have set the Planck area $A_0 = 4G$. Notice that when $\Delta = 0$, and $\bar{\beta} = 1$, the Λ CDM model is recovered.

Furthermore, the flatness constraint $E(0) = 1$, gives the equation

$$\Omega_{\Lambda0} = \left(\frac{2 + \Delta}{2 - \Delta} \right) \frac{1}{\bar{\beta}} - \Omega_{m0}. \quad (2.15)$$

In addition, the deceleration parameter is defined as

$$q = -1 - \frac{\dot{H}}{H^2}. \quad (2.16)$$

By substituting Eq. (2.13) and replacing Eqs. (2.6), (2.7) into (2.5), the $q(z)$ results

$$q(z) = -1 + \frac{3\Omega_{m0}(z+1)^3}{E(z)} \left[\frac{\bar{\beta}(2-\Delta)^{\Delta-1}}{(2+\Delta)} \right]^{1/(2-\Delta)} [\Omega_{m0}(z+1)^3 + \Omega_{\Lambda 0}]^{(\Delta-1)/(2-\Delta)}, \quad (2.17)$$

and the DE EoS in terms of Eqs. (2.13)-(2.14) is written as

$$w_{DE} = -1 + \frac{2(z+1)E(z)E'(z)[1 - (1 + \Delta/2)(E\bar{\beta})^{-\Delta}]}{3\Omega_{\Lambda} + 3E(z)^2 \left[1 - \frac{(2+\Delta)}{2-\Delta} (E\bar{\beta})^{-\Delta} \right]} \quad (2.18)$$

where

$$E'(z) = 3\Omega_{m0} \frac{\bar{\beta}}{2+\Delta} E(z)^{(\Delta-1)} (z+1)^2. \quad (2.19)$$

It is worthy to note that for $\bar{\beta} = 1$, $\Delta = 0$ and $z \rightarrow 1$ the EoS for the cosmological constant is recovered, i.e. $w_{DE} = -1$.

2.2 Model II: Matter, Radiation and Effective Dark Energy

By considering two fluids, matter and radiation, for a flat Universe, the Friedmann and Raychaudhuri equations in Barrow cosmology result as follows

$$H^2 = \frac{8\pi G}{3} (\rho_m + \rho_r + \rho_{DE}), \quad (2.20)$$

$$\dot{H} = -4\pi G (\rho_m + p_m + \rho_r + p_r + \rho_{DE} + p_{DE}), \quad (2.21)$$

where ρ_r indicates the radiation energy density and the radiation pressure is $p_r = \rho_r/3$. We define

$$\Omega_r \equiv \frac{8\pi G \rho_r}{3H^2}. \quad (2.22)$$

Using the previous variable definitions (2.11), the dimensionless Friedmann equation becomes

$$\Omega_{\Lambda} + \Omega_m + \Omega_r = \frac{\beta(\Delta+2)H^{-\Delta}}{2-\Delta}. \quad (2.23)$$

Finally, from Eq. (2.23) it follows

$$\Omega_m + \Omega_r + \Omega_{DE} = 1 + \underbrace{\Omega_m + \Omega_r + \Omega_{\Lambda} - \frac{\beta(\Delta+2)H^{-\Delta}}{2-\Delta}}_{=0} = 1. \quad (2.24)$$

The dimensionless Friedmann equation can be written as

$$E(z) \equiv \frac{H}{H_0} = \left\{ \bar{\beta} \frac{2-\Delta}{2+\Delta} [\Omega_{m0}(z+1)^3 + \Omega_{r0}(z+1)^4 + \Omega_{\Lambda 0}] \right\}^{1/(2-\Delta)}, \quad (2.25)$$

where the radiation component evolves in the traditional way $\rho_r = \rho_{r0}(z+1)^4$, and Ω_{r0} is obtained from (2.22) evaluated at $a = 1$ ($z = 0$). This can be calculated as $\Omega_{r0} = 2.469 \times 10^{-5} h^{-2} (1 + 0.2271 N_{eff})$, with $N_{eff} = 3.04$ as the number of relativistic species [26] and $h = H_0/100 \text{kms}^{-1} \text{Mpc}^{-1}$ as the current Hubble dimensionless parameter.

The flatness constricton $E(0) = 1$, gives the equation

$$\Omega_{\Lambda 0} = \left(\frac{2 + \Delta}{2 - \Delta} \right) \frac{1}{\bar{\beta}} - \Omega_{m0} - \Omega_{r0}. \quad (2.26)$$

In addition, the deceleration parameter reads

$$q(z) = -1 + \left[\frac{\bar{\beta}(2 - \Delta)^{\Delta-1}}{(2 + \Delta)} \right]^{1/(2-\Delta)} \times \frac{3\Omega_{m0}(z+1)^3 + 4\Omega_{r0}(z+1)^4}{E(z)} [\Omega_{m0}(z+1)^3 + \Omega_{r0}(z+1)^4 + \Omega_{\Lambda 0}]^{(\Delta-1)/(2-\Delta)}. \quad (2.27)$$

The DE EoS can be calculated by substituting Eq. (2.25) into Eq. (2.18) and $E'(z)$ as

$$E'(z) = \frac{\bar{\beta}}{2 + \Delta} E(z)^{(\Delta-1)} [3\Omega_{m0}(z+1)^2 + 4\Omega_{r0}(z+1)^3]. \quad (2.28)$$

Notice that for $\bar{\beta} = 1$, $\Delta = 0$ and $z \rightarrow 1$ the EoS for the cosmological constant is recovered.

3 Observational constraints

For both models under Barrow cosmology (Model I: universe filled by matter and Model II: universe filled by matter plus radiation), the free parameters of the model are: h , Ω_{m0} , $\bar{\beta}$, and Δ . To constrain these parameters we employ observational Hubble data (OHD) [27], Type Ia supernovae (SNIa) [28], HII galaxies (HIIG) [29], strong lensing systems (SLS) [30], and baryon acoustic oscillations (BAO) [31]. In the following we briefly describe these samples.

3.1 Observational Hubble Data

A cosmological-independent measurement of the Hubble parameter is acquired through the differential age (DA) technique [32] in cosmic chronometers (i.e passive elliptic galaxies). In this paper, we consider the OHD compilation provided by [27] containing 31 data points in the range $0.07 < z < 1.965$. Hence, the chi square function for OHD can be constructed through the following equation

$$\chi_{\text{OHD}}^2 = \sum_i^{31} \left(\frac{H_{th}(\Theta, z_i) - H_{obs}(z_i)}{\sigma_{obs}^i} \right)^2, \quad (3.1)$$

where $H_{th}(\Theta, z_i)$ and $H_{obs}(z_i)$, are the theoretical and observational Hubble parameters respectively at the redshift z_i , and σ_{obs}^i is the observational error. Notice that Θ is a vector related to the number of free parameters of the studied cosmological model.

3.2 Pantheon SNIa sample

The Pantheon sample [33] contains 1048 SNIa data points in the redshift range $0.001 < z < 2.3$. The observational distance modulus μ_{PAN} for Pantheon SNIa can be measured as

$$\mu_{\text{PAN}} = m_b^* - M_B + \alpha \times X_1 - \beta \times C + \Delta_M + \Delta_B, \quad (3.2)$$

where m_b^* corresponds to the observed peak magnitude, M_B is the B-band absolute magnitude, α , and β coefficients are nuisance parameters; X_1 and C are variables describing the time stretching of the light-curve and the Supernova color at maximum brightness, respectively. Δ_M is a distance correction based on the host-galaxy mass of the SNIa and Δ_B is a distance correction based on predicted biases from simulations.

The theoretical counterpart of the distance modulus for any cosmological model is given by $\mu_{th}(\Theta, z) = 5 \log_{10}(d_L(\Theta, z)/10\text{pc})$, where d_L is the luminosity distance given by

$$d_L(\Theta, z) = \frac{c}{H_0}(1+z) \int_0^z \frac{dz'}{E(z')}, \quad (3.3)$$

where c is the light speed velocity. Since that [33] provide $\tilde{\mu}_{\text{PAN}} = \mu_{\text{PAN}} + M_B$, we can marginalize over the M_B parameter to compare the data with the underlying cosmology. Thus, the marginalized figure-of-merit for the Pantheon sample is given by

$$\chi_{\text{Pan}M\text{marg}}^2 = a + \log\left(\frac{e}{2\pi}\right) - \frac{b^2}{e}, \quad (3.4)$$

where $a = \Delta\tilde{\mu}^T \cdot \mathbf{C}_{\mathbf{P}}^{-1} \cdot \Delta\tilde{\mu}$, $b = \Delta\tilde{\mu}^T \cdot \mathbf{C}_{\mathbf{P}}^{-1} \cdot \Delta\mathbf{1}$, $e = \Delta\mathbf{1}^T \cdot \mathbf{C}_{\mathbf{P}}^{-1} \cdot \Delta\mathbf{1}$, and $\Delta\tilde{\mu}$ is the vector of residuals between the model distance modulus and the observed $\tilde{\mu}_{\text{PAN}}$. The covariance matrix $\mathbf{C}_{\mathbf{P}}$ is constructed by adding the systematic and statistical matrices of $\tilde{\mu}_{\text{PAN}}$. We refer the interested reader to [33] for a detailed description of how these matrices are constructed.

3.3 HII Galaxies

HIIG are galaxies with large HII regions, product of young and hot stars (O and/or B type stars) ionizing the medium. For these galaxies there is a correlation between the measured luminosity, L , and the inferred velocity dispersion, σ , of the ionized gas. Several authors have shown that the correlation $L - \sigma$ could be used as a cosmological tracer [34–38, and references therein]. A HIIG data sample was compiled by [38] containing 107 low redshift ($0.0088 \leq z \leq 0.16417$) galaxies, and 46 high redshift ($0.636427 \leq z \leq 2.42935$) galaxies. [29] used such HIIG sample to constrain the cosmological parameters for six different cosmological models. Recently, [39] presented a new sample which contains 181 local and high- z HIIG data points in the redshift range $0.01 < z < 2.6$. In this paper, we use such HIIG sample, and follow their methodology [see 39].

The correlation between L and σ can be written as

$$\log L = \beta_{II} \log \sigma + \gamma, \quad (3.5)$$

where γ and β_{II} are the intercept and slope functions, respectively. Following [29, 38, 39], we set $\beta_{II} = 5.022$, and $\gamma = 33.268$. Therefore, the distance modulus takes the form

$$\mu_{obs} = 2.5 \log L - 2.5 \log f - 100.2, \quad (3.6)$$

where f is the flux emitted by the HIIG. Moreover, the theoretical distance modulus is

$$\mu_{th}(\Theta, z) = 5 \log d_L(\Theta, z) + 25, \quad (3.7)$$

being $d_L(\Theta, z)$ the luminosity distance (in Mpc).

The figure-of-merit is given by the following equation

$$\chi_{\text{HIIG}}^2 = \sum_i^{18} \frac{[\mu_{th}(\Theta, z_i) - \mu_{obs}(z_i)]^2}{\epsilon_i^2}, \quad (3.8)$$

where ϵ_i is the uncertainty of the i_{th} measurement and it can be calculated propagating the errors of Eq. 3.6 [see further details in 39].

3.4 Strong lensing systems

Several authors have shown that strong lensing systems can be used as cosmological tool to constrain cosmological parameters [30]. The method consists in comparing a theoretical distance ratio of angular diameter distances in the lens geometry with its observational counterpart. It can be obtained from the Einstein radius of a lens (modeled with a singular isothermal sphere) given by

$$\theta_E = 4\pi \frac{\sigma_l^2 D_{ls}}{c^2 D_s}, \quad (3.9)$$

where σ_l is the observed velocity dispersion of the lens galaxy, D_s is the angular diameter distance to the source at redshift z_s , and D_{ls} is the angular diameter distance from the lens (at redshift z_l) to the source. Then, the observational distance ratio of angular diameter distances is defined as

$$D^{obs} \equiv c^2 \theta_E / 4\pi \sigma^2. \quad (3.10)$$

To measure the theoretical distance ratio $D^{th}(\Theta, z_l, z_s) \equiv D_{ls}/D_s$, we calculate D_s using the definition of angular diameter distance of a source at redshift z

$$D_A(\Theta, z) = \frac{c}{H_0(1+z)} \int_0^z \frac{dz'}{E(z')}, \quad (3.11)$$

and D_{ls} through the definition of the angular diameter distance between two objects at redshift z_1 and z_2

$$D_{12}(\Theta, z) = \frac{c}{H_0(1+z_2)} \int_{z_1}^{z_2} \frac{dz'}{E(z')}. \quad (3.12)$$

The most recent compilation of Strong-Lensing Systems (SLS) given by [30] consists of 204 SLS spanning the redshift region $0.0625 < z_l < 0.958$ for the lens and $0.196 < z_s < 3.595$ for the source. To avoid convergence problems and discarding (unphysical) systems with $D_{ls} > D_s$, the authors provided a fiducial sample with an observational lens equation (D^{obs}) within the region $0.5 \leq D^{obs} \leq 1$.

In this work, we use such a fiducial sample consisting of 143 SLS, and the chi-square function takes the form

$$\chi_{\text{SLS}}^2 = \sum_i^{143} \frac{[D^{th}(\Theta, z_l, z_s) - D^{obs}(\theta_E, \sigma^2)]^2}{(\delta D^{obs})^2}, \quad (3.13)$$

where

$$\delta D^{obs} = D^{obs} \left[\left(\frac{\delta \theta_E}{\theta_E} \right)^2 + 4 \left(\frac{\delta \sigma}{\sigma} \right)^2 \right]^{1/2}, \quad (3.14)$$

being $\delta \theta_E$ and $\delta \sigma$ the uncertainties of the Einstein radius and velocity dispersion, respectively.

3.5 Baryon Acoustic Oscillations

BAO are considered as standard rulers, being primordial signatures of the interaction of baryons and photons in a hot plasma on the matter power spectrum in the pre-recombination epoch. Authors in [40] collected 6 correlated data points measured by [41–43]. To confront cosmological models to these data, it is useful to build the χ^2 -function in the form

$$\chi_{\text{BAO}}^2 = \Delta \vec{X}^T \text{Cov}^{-1} \Delta \vec{X}, \quad (3.15)$$

where $\Delta \vec{X}$ is the difference between the theoretical and observational values of $d_A(z_{\text{drag}})/D_V(z_i)$ where z_{drag} is defined by the sound horizon at baryon drag epoch measured at the redshift z_i , and Cov^{-1} is the inverse of covariance matrix, the dilation scale (D_V) is defined as [44]

$$D_V(\Theta, z) = \left[\frac{d_A^2(\Theta, z) c z}{H_0 E(z)} \right]^{1/3} \quad (3.16)$$

where $d_A(\Theta, z) = (1+z)D_A(\Theta, z)$ is the comoving angular-diameter distance and D_A is the angular diameter distance at z presented in Eq. (3.11). Additionally, r_{drag} is the sound horizon at baryon drag epoch. We use $r_{\text{drag}} = 147.21 \pm 0.23$ reported in [2].

3.6 Results from Observational constraints

The inference of the cosmological parameters under Barrow cosmology, for both model I (Eq. 2.13) and II (Eq. 2.25), is performed using a Bayesian Markov Chain Monte Carlo (MCMC) approach using the emcee Python module [45]. We set 3000 chains with 250 steps each one. The burn-in phase is stopped up to obtain convergence according to the auto-correlation time criteria. We build a Gaussian log-likelihood as the merit-of-function to minimize through the equation $-2 \log(\mathcal{L}_{\text{data}}) \propto \chi_{\text{data}}^2$ for each dataset, and consider Gaussian priors on h and Ω_{m0} centered at 0.6766 ± 0.0042 and 0.3111 ± 0.0056 [2], respectively, and a flat prior for Δ in the ranges: $\Delta : [0, 2]$. The parameter $\bar{\beta}$ is calculated using Eq. (2.14), where we have set $A_0 = 4G$. Additionally, a joint analysis can be constructed through the sum of their function-of-merits, i.e.,

$$\chi_{\text{Joint}}^2 = \chi_{\text{SNIa}}^2 + \chi_{\text{BAO}}^2 + \chi_{\text{OHD}}^2 + \chi_{\text{SLS}}^2 + \chi_{\text{HIIG}}^2, \quad (3.17)$$

where subscripts indicate the observational measurements under consideration.

Figure 1 shows the 2D confidence contours at 68% (1σ) and 99.7% (3σ) confidence level (CL) respectively, and 1D posterior distribution of the parameters in Barrow cosmology with a matter component (top panel) and matter plus radiation. In the case of the Δ parameter, although the contours for most of the samples are consistent with each other, the ones obtained using SLS data are in tension with those estimated with the other samples. However, this is not surprising inasmuch as reported by [30], the use of their fiduciary sample of 143 strong lensing systems while performs better constraining the cosmological models tested in such work (compared with other lensing samples), the parameters are not tightly constraint. Indeed, they reported that the range on the studied cosmological parameters were in agreement with those expected from other astrophysical observations, but they also discussed that the method needs improvement, in particular to take into account systematic biases (e.g. not fully confirmed lenses, multiple arcs, uncertain redshifts, complex lens substructure).

Table 1 presents the chi-square and mean values of the parameters obtained from the different data set and their uncertainties at 1σ for both Barrow cosmologies. We obtain

$\Delta = (5.912^{+3.353}_{-3.112}) \times 10^{-4}$, $\bar{\beta} = 0.920^{+0.042}_{-0.042}$, and $\Delta = (6.245^{+3.377}_{-3.164}) \times 10^{-4}$, $\bar{\beta} = 0.915^{+0.043}_{-0.043}$ for model I and II, respectively. Both models are consistent at 2σ with the standard cosmological model, i.e. $\Delta = 0$ and $\bar{\beta} = 1$. Moreover, the Δ bounds suggest the entropy-area relation is consistent with the Bekenstein entropy. From now on, we focus our discussion on the model II (matter and radiation components) since it is a more realistic model.

The top panel of the Figure 2 shows that the expansion rate estimated from the mean values of the Barrow cosmology parameters are consistent with the OHD. In addition, the reconstruction of the deceleration parameter as function of redshift is shown in the middle panel of Fig. 2. The $q(z)$ behavior is similar to the standard one, i.e. there is a transition at $z_t \simeq 0.711^{+0.035}_{-0.034}$ from a decelerated stage to an accelerated stage with $q_0 = -0.573^{+0.019}_{-0.019}$, suggesting a de Sitter solution. However, in the Barrow scenario the late cosmic acceleration is driven by the new terms in the dynamical equations. Finally, the bottom panel of Fig. 2 illustrates the reconstruction of the equation of state of the effective dark energy as function of redshift. It is worth noting that it has a transition at $z_{wde} \simeq 1.070^{+0.114}_{-0.104}$ from a quintessence-like regime to a phantom-like one, yielding $w_{DE}(0) \simeq -1.000134^{+0.000069}_{-0.000068}$ at current times, which is consistent with the cosmological constant at 1σ . This behavior of $w_{DE}(z)$ has been also discussed by [20], the effective dark energy can undergo the phantom-divide crossing but it tends asymptotically to a de Sitter solution at late times.

Furthermore, the age of the Universe can be estimated by solving the integral $t_0 = \int_0^1 da/aH(a)$. Considering the constraints from the joint analysis, we obtain $t_0 \simeq 14.062^{+0.179}_{-0.170}$ ($14.045^{+0.179}_{-0.167}$) Gyr for matter+radiation (matter) model, consistent with 2σ confidence level with the measurements of Planck [2]. Thus, the constraints obtained from several data at different scales indicate that, by modifying the entropy-area relation, Barrow cosmology is a plausible scenario to explain the late cosmic acceleration without the need to include an exotic component.

In the following sections, we perform a dynamical system analysis of the Barrow cosmology.

4 Dynamical system and stability analysis

The phase-space and stability analysis is a complementary inspection that allows us to obtain a qualitative description of the local and global dynamics of cosmological scenarios independent of the initial conditions and the specific evolution of the universe. Furthermore, one can find asymptotic solutions and the corresponding theoretical values to compare with the observable ones. Examples of such quantities are the DE and total equation-of-state parameters, the deceleration parameter, the density parameters for the different species, etc. These observables allow to classify the cosmological solutions. In this regard, we can follow the reference [46], the first book related to modern dynamical systems theory to both cosmological models and observations.

In order to perform the stability analysis of a given cosmological scenario, one first transforms it to its autonomous form $\mathbf{X}' = \mathbf{f}(\mathbf{X})$ [46–54], where \mathbf{X} is a column vector containing some auxiliary variables and primes denote derivative with respect to a time variable (conveniently chosen). Then, one extracts the critical points \mathbf{X}_c by imposing the condition $\mathbf{X}' = \mathbf{0}$ and, in order to determine their stability properties, one expands around them with \mathbf{U} the column vector of the perturbations of the variables. Therefore, for each critical point the perturbation equations are expanded to first order as $\mathbf{U}' = \mathbf{Q} \cdot \mathbf{U}$, with the matrix \mathbf{Q}

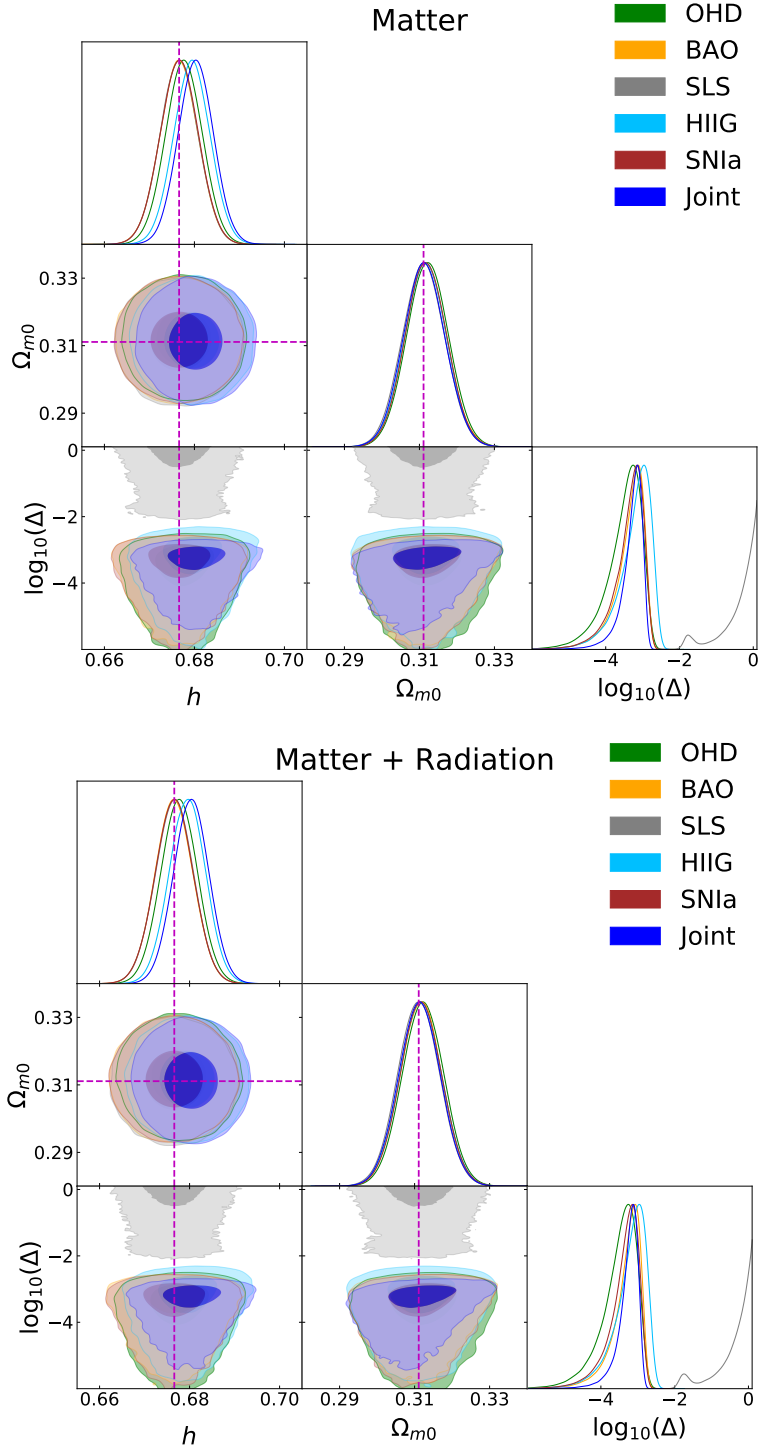


Figure 1. 2D contour at 68% and 99.7% CL and 1D posterior distribution of the free parameters in two models: universe filled by matter (top panel) and universe filled by matter plus radiation (bottom panel). Dashed lines represent best-fit values for Λ CDM [2].

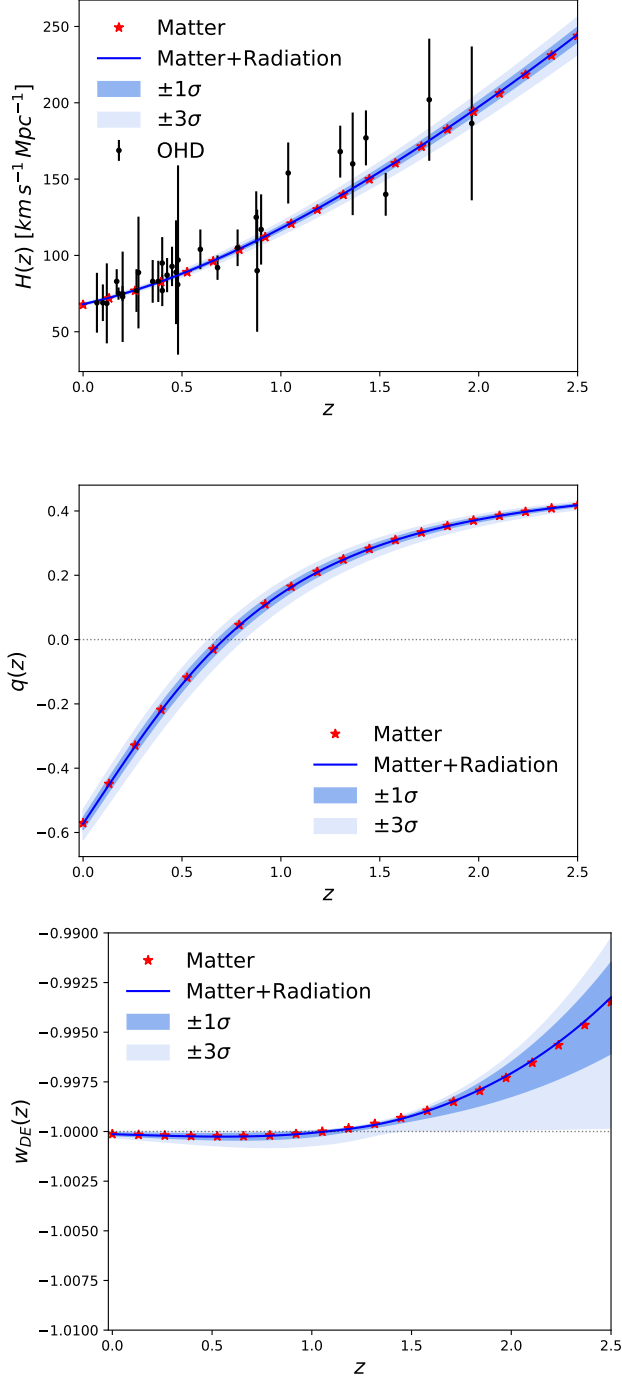


Figure 2. Top panel: $H(z)$ function for the Barrow cosmological model using the mean values of the joint analysis. Middle panel: Reconstruction of the cosmological evolution of $q(z)$ function using the mean values of the joint analysis. Bottom panel : Reconstruction of the equation-of-state of the effective dark energy. In all panels the shadow regions represent the 1σ , and 3σ (from darker to lighter color bands) confidence levels.

Table 1. Mean values of the free parameters for the Barrow cosmology in two scenarios: universe filled by matter (Model I) and by matter plus radiation (Model II).

Sample	χ^2	h	$\Omega_m^{(0)}$	Δ
Model I				
SLS	217.28	$0.677^{+0.004}_{-0.004}$	$0.311^{+0.006}_{-0.006}$	$0.963^{+0.704}_{-0.700}$
BAO	2.97	$0.677^{+0.004}_{-0.004}$	$0.312^{+0.006}_{-0.005}$	$(5.370^{+4.713}_{-3.550}) \times 10^{-4}$
DA OHD	15.62	$0.678^{+0.004}_{-0.004}$	$0.312^{+0.006}_{-0.006}$	$(3.813^{+4.774}_{-2.752}) \times 10^{-4}$
HII	441.64	$0.679^{+0.004}_{-0.004}$	$0.312^{+0.005}_{-0.006}$	$(7.548^{+8.094}_{-5.272}) \times 10^{-4}$
SNIa	1036.11	$0.677^{+0.004}_{-0.004}$	$0.312^{+0.005}_{-0.005}$	$(5.056^{+4.678}_{-3.361}) \times 10^{-4}$
Joint	1749.08	$0.680^{+0.004}_{-0.004}$	$0.311^{+0.006}_{-0.005}$	$(5.912^{+3.353}_{-3.112}) \times 10^{-4}$
Model II				
SLS	217.28	$0.677^{+0.004}_{-0.004}$	$0.311^{+0.006}_{-0.006}$	$0.963^{+0.703}_{-0.708}$
BAO	2.86	$0.677^{+0.004}_{-0.004}$	$0.312^{+0.005}_{-0.006}$	$(6.008^{+4.949}_{-3.880}) \times 10^{-4}$
DA OHD	15.61	$0.678^{+0.004}_{-0.004}$	$0.312^{+0.006}_{-0.006}$	$(3.809^{+4.855}_{-2.740}) \times 10^{-4}$
HII	441.64	$0.680^{+0.004}_{-0.004}$	$0.312^{+0.006}_{-0.006}$	$(7.540^{+8.107}_{-5.245}) \times 10^{-4}$
SNIa	1036.11	$0.677^{+0.004}_{-0.004}$	$0.312^{+0.006}_{-0.005}$	$(5.105^{+4.680}_{-3.383}) \times 10^{-4}$
Joint	1748.89	$0.680^{+0.004}_{-0.004}$	$0.311^{+0.006}_{-0.006}$	$(6.245^{+3.377}_{-3.164}) \times 10^{-4}$

containing the coefficients of the perturbation equations. The eigenvalues of \mathbf{Q} determine the type and stability of the specific critical point.

4.1 Stability analysis of Model I

To start the dynamical analysis for the Barrow cosmology (§2), we use the dynamical variables $(\Omega_m, \Omega_\Lambda)$ defined in (2.11), say,

$$\Omega_m = \frac{8\pi G\rho_m}{3H^2}, \quad \Omega_\Lambda = \frac{\Lambda}{3H^2}. \quad (4.1)$$

As we commented before, the normalized Friedmann equation (2.9) is then transformed to

$$\Omega_\Lambda + \Omega_m = \frac{\beta(\Delta + 2)H^{-\Delta}}{2 - \Delta}. \quad (4.2)$$

Notice that by substituting $\beta = 1, \Delta = 0$, in Eq. (2.9), we obtain the usual relation in FRW cosmology. For $\beta \neq 1, \Delta \neq 0$, by substituting Eqs. (2.6) and (2.7) into Eq. (2.5), we obtain

$$8\pi G\rho_m + \beta(\Delta + 2)H^{-\Delta}\dot{H} = 0, \quad (4.3)$$

$$\implies 3H^2\Omega_m + \beta(\Delta + 2)H^{-\Delta}\dot{H} = 0, \quad (4.4)$$

$$\implies 3H^2\Omega_m + (2 - \Delta)(\Omega_\Lambda + \Omega_m)\dot{H} = 0. \quad (4.5)$$

Then, for $H \neq 0, \beta \neq 1$, and $\Delta \neq 0$, the deceleration parameter (Eq. (2.16)) results

$$q = -1 + \frac{3\Omega_m}{(2 - \Delta)(\Omega_\Lambda + \Omega_m)}, \quad (4.6)$$

for Λ CDM ($\beta = 1, \Delta = 0$) we obtain the usual relation $q = -1 + \frac{3}{2}\Omega_m$.

In general, $H(t)$ satisfies the differential equation

$$\dot{H} = \frac{\Lambda H^\Delta}{\beta(\Delta + 2)} + \frac{3H^2}{\Delta - 2}. \quad (4.7)$$

Furthermore, we have

$$\rho_m = -\frac{3\beta(\Delta + 2)H^{2-\Delta}}{8\pi(\Delta - 2)G} - \frac{\Lambda}{8\pi G}. \quad (4.8)$$

Finally, we obtain the dynamical system

$$\Omega'_\Lambda = 2(q + 1)\Omega_\Lambda, \quad \Omega'_m = (2q - 1)\Omega_m, \quad (4.9)$$

where the prime means derivative with respect $\tau = \ln(a)$, and q is defined by (4.6). The main difference with the Λ CDM model is that the term $\frac{\beta(\Delta+2)H^{-\Delta}}{2-\Delta}$ in Eq. (4.2) is unbounded as $H \rightarrow 0$, resulting in unbounded Ω_Λ, Ω_m . The equilibrium points in the finite part of the phase space are

1. the line $A(\Omega_\Lambda) : \Omega_m = 0, \Omega_\Lambda = \text{arbitrary}$, for $\Delta = \text{arbitrary}$, with eigensystem $\begin{pmatrix} 0 & -3 \\ \{1, 0\} & \{\frac{2}{\Delta-2}, 1\} \end{pmatrix}$; and
2. the line $B(\Omega_m) : \Omega_m = \text{arbitrary}, \Omega_\Lambda = 0$, for $\Delta = 0$, with eigensystem $\begin{pmatrix} 3 & 0 \\ \{-1, 1\} & \{0, 1\} \end{pmatrix}$.

The line of points $B(\Omega_m)$ exists only for $\Delta = 0$. All these lines of equilibrium points are normally hyperbolic because the tangent vector at a given point of each line is parallel to the corresponding eigenvector associated to the zero eigenvalue. This implies that the stability conditions can be inferred from the eigenvalues with non-zero real parts [55]. Therefore, the line $A(\Omega_\Lambda)$ is the attractor of the system, representing de Sitter solutions. For $\Delta = 0$, the line $B(\Omega_m)$ contains the past attractors, which represents matter dominated solutions.

4.1.1 Global dynamical systems formulation

In this section we define the compact variables (assuming $H \geq 0, H_0 > 0$) based on the approach by [56]:

$$T = \frac{H_0}{H_0 + H}, \quad (4.10)$$

along with the angular variable

$$\theta = \tan^{-1} \left(\sqrt{\frac{\Omega_m}{\Omega_\Lambda}} \right) = \tan^{-1} \left(\sqrt{\frac{8\pi G \rho_m}{\Lambda}} \right), \quad (4.11)$$

with inverse

$$H = \frac{H_0(1 - T)}{T}, \quad \rho_m = \frac{\Lambda \tan^2(\theta)}{8\pi G}. \quad (4.12)$$

We obtain the dynamical system

$$\begin{aligned} \frac{dT}{d\bar{\tau}} &= -\frac{3(1-T)^2 T}{\Delta - 2} - \frac{\Lambda T^3 H_0^{\Delta-2} \left(\frac{1}{T} - 1\right)^\Delta}{\beta(\Delta + 2)}, \\ \frac{d\theta}{d\bar{\tau}} &= -\frac{3}{4}(1-T) \sin(2\theta), \end{aligned} \quad (4.13)$$

Label	Coordinates	Eigenvalues	Stability
dS_+	$\{\theta = 2n\pi\}$	$\left\{-\frac{3}{2}, 0\right\}$	sink
dS_-	$\{\theta = (2n+1)\pi\}$	$\left\{-\frac{3}{2}, 0\right\}$	sink
$M_-^{(0)}$	$\{T = 0, \theta = (4n-1)\frac{\pi}{2}\}$	$\left\{\frac{3}{2-\Delta}, \frac{3}{2}\right\}$	source
$M_+^{(0)}$	$\{T = 0, \theta = (4n+1)\frac{\pi}{2}\}$	$\left\{\frac{3}{2-\Delta}, \frac{3}{2}\right\}$	source
$M_-^{(1)}$	$\{T = 1, \theta = (4n-1)\frac{\pi}{2}\}$	$\left\{-\frac{3}{2-\Delta}, \frac{3}{2}\right\}$	saddle
$M_+^{(1)}$	$\{T = 1, \theta = (4n+1)\frac{\pi}{2}\}$	$\left\{-\frac{3}{2-\Delta}, \frac{3}{2}\right\}$	saddle

Table 2. Equilibrium points/lines of system (4.16).

where for a function $f \in \{T, \theta\}$ we have introduced the new derivative

$$\frac{df}{d\bar{\tau}} = \frac{1}{(H_0 + H)} \frac{df}{dt},$$

which allows for a global dynamical system analysis.

On the other hand, the equation (4.2) leads to

$$\frac{\Lambda T^2 \sec^2(\theta)}{3H_0^2(1-T)^2} + \frac{\beta(\Delta+2)(H_0(\frac{1}{T}-1))^{-\Delta}}{\Delta-2} = 0, \quad (4.14)$$

that can be solved globally for β , and we end up with the system

$$\begin{aligned} \frac{dT}{d\bar{\tau}} &= \frac{3(1-T)^2 T \sin^2(\theta)}{2-\Delta}, \\ \frac{d\theta}{d\bar{\tau}} &= -\frac{3}{4}(1-T) \sin(2\theta), \end{aligned} \quad (4.15)$$

defined in the finite cylinder \mathbf{S} with boundaries $T = 0$ and $T = 1$, where the power-law dependence in the first equation (4.13) is eliminated. Using the logarithmic variable $\tau = \ln(a)$, we obtain the complementary system

$$\begin{aligned} \frac{dT}{d\tau} &= \frac{3(1-T)T \sin^2(\theta)}{2-\Delta}, \\ \frac{d\theta}{d\tau} &= -\frac{3}{4} \sin(2\theta). \end{aligned} \quad (4.16)$$

The deceleration parameter is now written as

$$q = -1 + \frac{3\Omega_m}{(2-\Delta)\Omega_\Lambda \left(\frac{\Omega_m}{\Omega_\Lambda} + 1\right)} = -1 + \frac{3 \sin^2(\theta)}{2-\Delta}. \quad (4.17)$$

From the first equation in (4.16), T is a monotonically increasing function on \mathbf{S} . As a consequence, all orbits originate from the invariant subset $T = 0$ (which contains the α -limit), which is classically related to the initial singularity with $H \rightarrow \infty$, and ends on the invariant boundary subset $T = 1$, which corresponds asymptotically to $H = 0$.

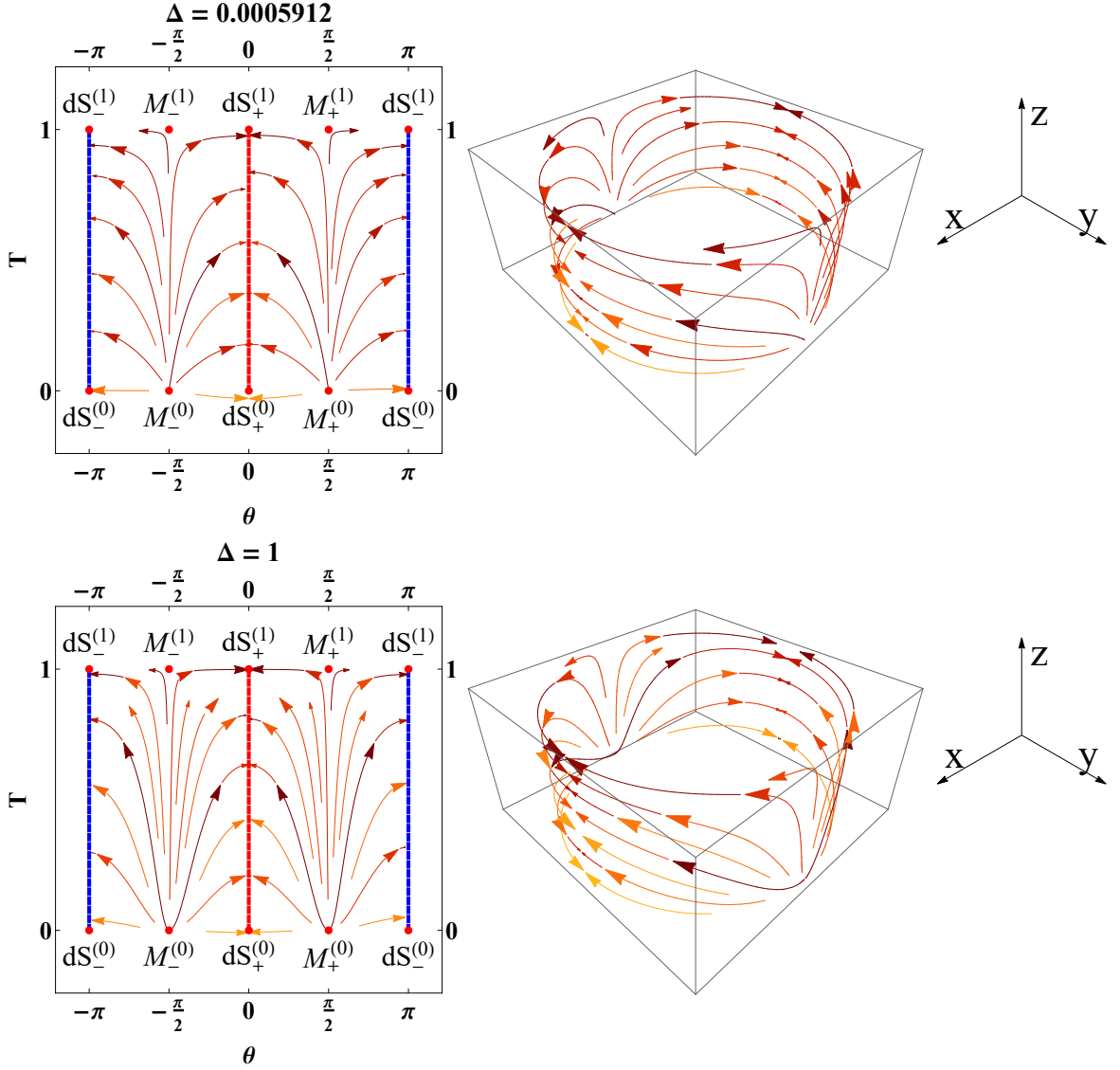


Figure 3. Unwrapped solution space (left panel) and projection over the cylinder \mathbf{S} defined in Cartesian coordinates (x, y, z) by (4.20) (right panel) of the solution space of system (4.15) for $\Delta = 5.912 \times 10^{-4}$, $\bar{\beta} = 0.920$ (top panel) and $\Delta = 1$, $\bar{\beta} = 1$ (bottom panel).

We have the relations for the fractional energy densities:

$$\Omega_m = \frac{\beta(\Delta + 2)H_0^{1-\Delta} \left(\frac{1}{T} - 1\right)^{1-\Delta}}{2(2 - \Delta)} - \frac{\Lambda T}{6H_0(1 - T)}, \quad (4.18)$$

$$\Omega_\Lambda = \frac{\Lambda T}{6H_0(1 - T)}. \quad (4.19)$$

The system (4.16) admits the equilibrium points summarized in Table 2:

1. $M_\pm^{(0)} : \theta = (4n \pm 1)\frac{\pi}{2}, T = 0$, represented in Fig. 3;

2. $M_{\pm}^{(1)} : \theta = (4n \pm 1)\frac{\pi}{2}, T = 1$, represented in Fig. 3;
3. $dS_+ : \theta = 2n\pi, T = \text{arbitrary}$, with representatives $dS_+^{(0)}$ and $dS_+^{(1)}$ respectively, denoted in Fig. 3 by a red line;
4. $dS_- : \theta = (2n + 1)\pi, T = \text{arbitrary}$, with representatives $dS_-^{(0)}$ and $dS_-^{(1)}$ respectively, denoted in Fig. 3 by a blue line;

where n is an integer. There are two equivalent (due to the discrete symmetry) hyperbolic fixed points M_{\pm} for which $q = -1 + \frac{3}{2-\Delta}$, i.e. they are associated with dust fluid for $\Delta = 0$, and two equivalent fixed points dS_{\pm} for which $q = -1$, which therefore correspond to a de Sitter state.

For a representation of the flow of (4.16), we integrate it in the variables T, θ and project in a compact set using the ‘‘cylinder-adapted’’ coordinates

$$\mathbf{S} : \begin{cases} x = \cos \theta, \\ y = \sin \theta, \\ z = T, \end{cases} \quad (4.20)$$

with $0 \leq T \leq 1, \theta_1 \in [-\pi, \pi]$, with inverse

$$\begin{cases} \theta = \tan^{-1}\left(\frac{y}{x}\right), \\ T = z. \end{cases} \quad (4.21)$$

Also, we present the whole evolution in the space (Ω_m, T) through the transform $(T, \theta) \mapsto (\Omega_m, T)$ where

$$\Omega_m = \left[\left(\frac{2 + \Delta}{2 - \Delta} \right) \frac{1}{\bar{\beta}} - \Omega_{m0} \right] \frac{T^2}{(1 - T)^2} \tan^2(\theta). \quad (4.22)$$

The value $T = 1/2$ corresponds to current time. In these variables we have the system

$$\begin{aligned} \frac{d\Omega_m}{d\tau} &= \frac{3\Omega_m (\bar{\beta} ((\Delta - 2)T^2\Omega_{m0} - \Delta(1 - T)^2\Omega_m) + (\Delta + 2)T^2)}{(\Delta - 2)\bar{\beta} ((1 - T)^2\Omega_m - T^2\Omega_{m0}) - (\Delta + 2)T^2}, \\ \frac{dT}{d\tau} &= \frac{3(T - 1)^3 T \bar{\beta} \Omega_m}{(\Delta - 2)\bar{\beta} ((1 - T)^2\Omega_m - T^2\Omega_{m0}) - (\Delta + 2)T^2}. \end{aligned} \quad (4.23)$$

In Figure 3 are represented the streamlines of the flow of (4.15) onto the unwrapped solution space (left panel) and its projection over the cylinder \mathbf{S} (right panel) for two values of Δ one obtained from the joint constraint $\Delta = 5.912 \times 10^{-4}$, and the other one is the extreme value $\Delta = 1$. The phase space is qualitatively the same as for system (4.16). Firstly, observe that systems (4.15) and (4.16) are independent of $\bar{\beta}$. Therefore, the parameter $\bar{\beta}$ is dynamically irrelevant. The results summarized in points 1-4 before are confirmed in Figure 3. That is, the matter dominated solutions $M_{\pm}^{(0)} : \theta = (4n \pm 1)\frac{\pi}{2}, T = 0$ ($H \rightarrow \infty$) are past attractors. The matter dominated solutions $M_{\pm}^{(1)} : \theta = (4n \pm 1)\frac{\pi}{2}, T = 1$ ($H \rightarrow 0$) are saddle and the attractor is the line of equilibrium points connecting $dS_-^{(0)}$ and $dS_-^{(1)}$ which are de Sitter solutions.

In Figure 4 streamlines of the flow of (4.23) are presented. We select the parameters (a) $\Delta = 5.912 \times 10^{-4}, \bar{\beta} = 0.920, \Omega_{m0} = 0.311$ obtained from the joint constraints and (b)

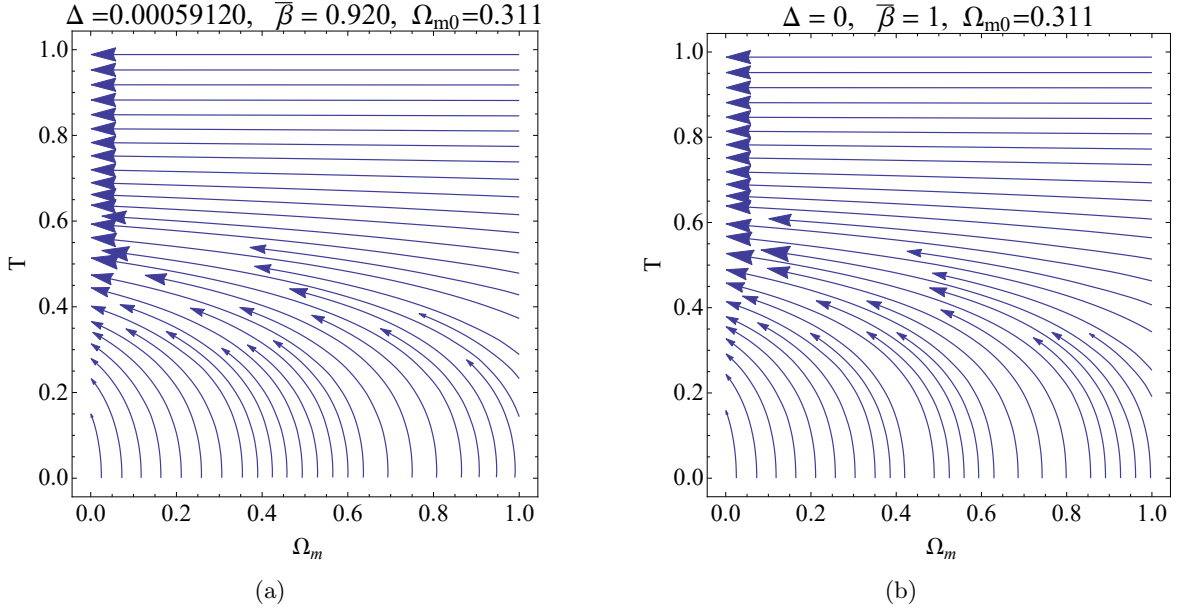


Figure 4. Streamlines of the flow of (4.23) for (a) $\Delta = 5.912 \times 10^{-4}, \bar{\beta} = 0.920, \Omega_{m0} = 0.311$ obtained from the joint constraints and (b) $\Delta = 0, \beta = 1, \Omega_{m0} = 0.311$ obtained from Λ CDM model.

$\Delta = 0, \beta = 1, \Omega_{m0} = 0.311$ for Λ CDM model. These plots confirms that the late time attractor is the line of de Sitter points dS_+ and dS_- .

Complementary, we define an unbounded variable \tilde{T} and keep θ :

$$\tilde{T} = \frac{H_0}{H}, \quad \theta = \tan^{-1} \left(\sqrt{\frac{8\pi G \rho_m}{\Lambda}} \right), \quad (4.24)$$

and using the logarithmic variable $\tau = \ln(a) = -\ln(1+z)$, we obtain the complementary system

$$\begin{aligned} \frac{d\tilde{T}}{d\tau} &= \frac{3\tilde{T} \sin^2(\theta)}{2 - \Delta}, \\ \frac{d\theta}{d\tau} &= -\frac{3}{4} \sin(2\theta). \end{aligned} \quad (4.25)$$

Setting $a = 1$ for the current universe, and considering the initial conditions:

$$\theta(0) = \tan^{-1} \left(\sqrt{\frac{\Omega_{m0}}{\Omega_{\Lambda 0}}} \right), \quad \tilde{T}(0) = 1, \quad (4.26)$$

the system (4.25) is integrated to obtain

$$\theta(\tau) = \tan^{-1} \left(e^{-3\tau/2} \sqrt{\frac{\Omega_{m0}}{\Omega_{\Lambda 0}}} \right), \quad (4.27)$$

$$\tilde{T}(\tau) = e^{-\frac{3\tau}{\Delta-2}} \left(\frac{\Omega_{\Lambda 0} + \Omega_{m0}}{\Omega_{\Lambda 0}} \right)^{\frac{1}{2-\Delta}} \left(e^{3\tau} + \frac{\Omega_{m0}}{\Omega_{\Lambda 0}} \right)^{\frac{1}{\Delta-2}}, \quad (4.28)$$

Finally, we get the exact evolution of H and ρ_m :

$$\begin{aligned} H &= H_0 e^{-\frac{3\tau}{2-\Delta}} \left(\frac{\Omega_{\Lambda 0}}{\Omega_{\Lambda 0} + \Omega_{m 0}} \right)^{\frac{1}{2-\Delta}} \left(e^{3\tau} + \frac{\Omega_{m 0}}{\Omega_{\Lambda 0}} \right)^{\frac{1}{2-\Delta}} \\ &= H_0 \left(\frac{\Omega_{m 0}(z+1)^3 + \Omega_{\Lambda 0}}{\Omega_{\Lambda 0} + \Omega_{m 0}} \right)^{\frac{1}{2-\Delta}}, \end{aligned} \quad (4.29)$$

$$\rho_m = \frac{\Lambda \tan^2(\theta)}{8\pi G} = \frac{\Lambda e^{-3\tau} \Omega_{m 0}}{8\pi G \Omega_{\Lambda 0}} = \frac{3H_0^2 \Omega_{m 0}}{8\pi G} (z+1)^3. \quad (4.30)$$

Eq. (4.29) can be deduced from Eq. (2.13) after the substitution of $\left(\frac{2+\Delta}{2-\Delta}\right) \frac{1}{\beta}$ from Eq. (2.15).

These expressions are used to obtain the fractional energy densities corresponding to matter, to an effective Λ -like source, and to the effective dark energy as follows:

$$\Omega_m(z) = \frac{8\pi G \rho_m}{3H^2} = \Omega_{m 0}(z+1)^3 \left(\frac{\Omega_{m 0}(z+1)^3 + \Omega_{\Lambda 0}}{\Omega_{\Lambda 0} + \Omega_{m 0}} \right)^{-\frac{2}{2-\Delta}}, \quad (4.31)$$

and

$$\Omega_{\Lambda}(z) = \frac{\Lambda}{3H^2} = \Omega_{\Lambda 0} \left(\frac{\Omega_{m 0}(z+1)^3 + \Omega_{\Lambda 0}}{\Omega_{\Lambda 0} + \Omega_{m 0}} \right)^{-\frac{2}{2-\Delta}}, \quad \Omega_{\Lambda 0} = \frac{\Lambda}{3H_0^2}. \quad (4.32)$$

From Eq. (2.6) we infer

$$\begin{aligned} \Omega_{DE}(z) &= \frac{8\pi G \rho_{DE}}{3H^2} = \frac{\Lambda}{3H^2} + \left[1 - \frac{\beta(\Delta+2)}{2-\Delta} H^{-\Delta} \right] \\ &= 1 + \Omega_{\Lambda} - \frac{\beta(\Delta+2)}{2-\Delta} H_0^{-\Delta} \left(\frac{\Omega_{m 0}(z+1)^3 + \Omega_{\Lambda 0}}{\Omega_{\Lambda 0} + \Omega_{m 0}} \right)^{-\frac{\Delta}{2-\Delta}} \\ &= 1 + \Omega_{\Lambda 0} \left(\frac{\Omega_{m 0}(z+1)^3 + \Omega_{\Lambda 0}}{\Omega_{\Lambda 0} + \Omega_{m 0}} \right)^{-\frac{2}{2-\Delta}} - \frac{(\Delta+2)}{(2-\Delta)} \frac{1}{\beta} \left(\frac{\Omega_{m 0}(z+1)^3 + \Omega_{\Lambda 0}}{\Omega_{\Lambda 0} + \Omega_{m 0}} \right)^{-\frac{\Delta}{2-\Delta}} \\ &= 1 + \Omega_{\Lambda 0} \left(\frac{\Omega_{m 0}(z+1)^3 + \Omega_{\Lambda 0}}{\Omega_{\Lambda 0} + \Omega_{m 0}} \right)^{-\frac{2}{2-\Delta}} - (\Omega_{\Lambda 0} + \Omega_{m 0}) \left(\frac{\Omega_{m 0}(z+1)^3 + \Omega_{\Lambda 0}}{\Omega_{\Lambda 0} + \Omega_{m 0}} \right)^{-\frac{\Delta}{2-\Delta}} \\ &= 1 - \Omega_{m 0}(1+z)^3 \left(\frac{\Omega_{m 0}(1+z)^3 + \Omega_{\Lambda 0}}{\Omega_{\Lambda 0} + \Omega_{m 0}} \right)^{-\frac{2}{2-\Delta}} \end{aligned} \quad (4.33)$$

where we use Eq. (2.15) to eliminate the term $\left(\frac{2+\Delta}{2-\Delta}\right) \frac{1}{\beta}$, apply $-\frac{\Delta}{2-\Delta} = 1 - \frac{2}{2-\Delta}$, and algebraically manipulate the equations to obtain $\Omega_{DE} = 1 - \Omega_m$. It is straightforward to infer Eqs. (4.31), (4.32) and (4.33) in terms of the scale factor by replacing $z = (1/a) - 1$.

Figure 5 shows the evolution of the density parameters Ω_m and Ω_{DE} as a function of the scale factor a for two cases: the joint constraints for h , $\Omega_{m 0}$, Δ and β presented in Table 1 (solid lines) and the values for the standard model $\Delta = 0$, $\beta = 1$ (dashed lines). The shadowed regions represent the 3σ confidence levels. It is worthy to note that there are values of the energy densities which satisfy $\Omega_m > 1$ and $\Omega_{DE} < 0$, however, these values are close to Λ CDM lines within the 3σ error propagation.

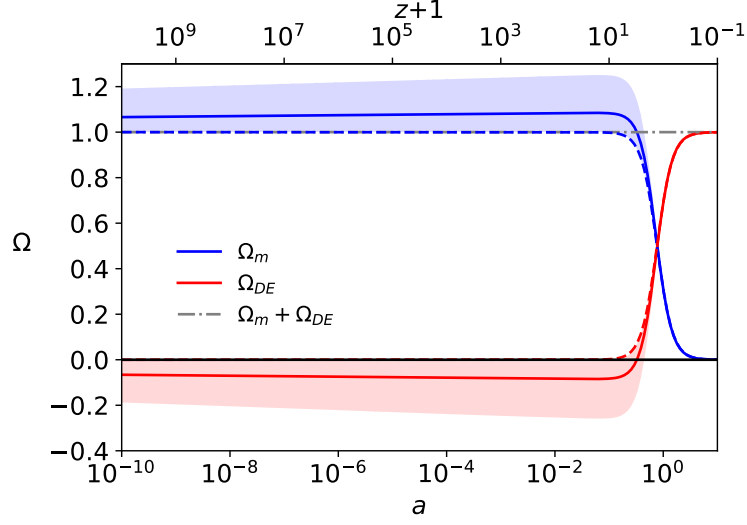


Figure 5. Evolution of the density parameters for matter and effective dark energy in Barrow Cosmology using the joint constraints (solid lines) and the standard model ($\Delta = 0$, and $\bar{\beta} = 1$, dashed lines). The shadow regions represent the 3σ confidence levels.

4.2 Stability analysis of Model II

We start our stability study of the dynamical variables (2.11) and (2.22), say,

$$\Omega_m = \frac{8\pi G\rho_m}{3H^2}, \quad \Omega_r = \frac{8\pi G\rho_r}{3H^2}, \quad \Omega_\Lambda = \frac{\Lambda}{3H^2}, \quad (4.34)$$

related by (2.23). The evolution equations are now given by

$$\begin{aligned} \Omega'_\Lambda &= 2(q+1)\Omega_\Lambda, \\ \Omega'_m &= (2q-1)\Omega_m, \\ \Omega'_r &= 2(q-1)\Omega_r, \end{aligned} \quad (4.35)$$

where the prime means derivative with respect to $\tau = \ln(a)$, and q is defined by (4.36)

$$q = -1 + \frac{3\Omega_m + 4\Omega_r}{(2-\Delta)(\Omega_\Lambda + \Omega_m + \Omega_r)}. \quad (4.36)$$

The equilibrium points in the finite part of the phase space are the lines of equilibrium points:

1. the line $A(\Omega_\Lambda) : \Omega_m = 0, \Omega_r, \Omega_\Lambda = \text{arbitrary}$, for $\Delta = \text{arbitrary}$, with eigensystem $\begin{pmatrix} 0 & -4 & -3 \\ \{1, 0, 0\} & \left\{ \frac{2}{\Delta-2}, 0, 1 \right\} & \left\{ \frac{2}{\Delta-2}, 1, 0 \right\} \end{pmatrix}$;
2. the line $B(\Omega_m) : \Omega_m = \text{arbitrary}, \Omega_r = 0, \Omega_\Lambda = 0$, for $\Delta = 0$, with eigensystem $\begin{pmatrix} 3 & -1 & 0 \\ \{-1, 1, 0\} & \{0, -1, 1\} & \{0, 1, 0\} \end{pmatrix}$; and
3. the line $C(\Omega_r) : \Omega_m = 0, \Omega_r = \text{arbitrary}, \Omega_\Lambda = 0$, for $\Delta = 0$, with eigensystem $\begin{pmatrix} 4 & 1 & 0 \\ \{-1, 0, 1\} & \{0, -1, 1\} & \{0, 0, 1\} \end{pmatrix}$.

The last two lines of equilibrium points, $B(\Omega_m)$ and $C(\Omega_r)$, exist only for $\Delta = 0$. All three lines are normally hyperbolic because the tangent vector at a given point of each line is parallel to the corresponding eigenvector associated to the zero eigenvalue. This implies that the stability conditions can be inferred from the eigenvalues with non-zero real parts [55]. Therefore, the line $A(\Omega_\Lambda)$ is the attractor of the system, representing de Sitter solutions. For $\Delta = 0$, the line $B(\Omega_m)$ is a saddle, representing matter dominated solutions, and the line $C(\Omega_r)$ contains the past attractors, which represents radiation dominated solutions.

4.2.1 Global dynamical systems formulation

In this section we define the compact variable (assuming $H \geq 0, H_0 > 0$) based on the approach by [56]:

$$T = \frac{H_0}{H_0 + H}, \quad (4.37)$$

along with the angular ones

$$\theta_1 = \tan^{-1} \left(\sqrt{\frac{8\pi G \rho_m}{\Lambda}} \right), \quad \theta_2 = \tan^{-1} \left(\sqrt{\frac{8\pi G \rho_r}{\Lambda}} \right), \quad (4.38)$$

with inverse

$$H = \frac{H_0(1-T)}{T}, \quad \rho_m = \frac{\Lambda \tan^2(\theta_1)}{8\pi G}, \quad \rho_r = \frac{\Lambda \tan^2(\theta_2)}{8\pi G}. \quad (4.39)$$

Furthermore, we have

$$\beta = \frac{(2-\Delta)\Lambda T^2 (\tan^2(\theta_1) + \tan^2(\theta_2) + 1) (H_0 (\frac{1}{T} - 1))^\Delta}{3(\Delta+2)H_0^2(1-T)^2}, \quad (4.40)$$

and

$$q = -1 + \frac{3 \tan^2(\theta_1) + 4 \tan^2(\theta_2)}{(2-\Delta) (\tan^2(\theta_1) + \tan^2(\theta_2) + 1)} \quad (4.41)$$

We obtain the dynamical system

$$\begin{aligned} \frac{dT}{d\bar{\tau}} &= \frac{(1-T)^2 T (3 \tan^2(\theta_1) + 4 \tan^2(\theta_2))}{(2-\Delta) (\tan^2(\theta_1) + \tan^2(\theta_2) + 1)}, \\ \frac{d\theta_1}{d\bar{\tau}} &= -\frac{3}{4}(1-T) \sin(2\theta_1), \\ \frac{d\theta_2}{d\bar{\tau}} &= -(1-T) \sin(2\theta_2), \end{aligned} \quad (4.42)$$

where for any function $f \in \{T, \theta_1, \theta_2\}$ we have introduced the new derivative

$$\frac{df}{d\bar{\tau}} = \frac{1}{(H_0 + H)} \frac{df}{dt},$$

which allows for a global dynamical system analysis.

Using the logarithmic variable $\tau = \ln(a)$, we get the complementary system

$$\begin{aligned} \frac{dT}{d\tau} &= \frac{(1-T)T (3 \tan^2(\theta_1) + 4 \tan^2(\theta_2))}{(2-\Delta) (\tan^2(\theta_1) + \tan^2(\theta_2) + 1)}, \\ \frac{d\theta_1}{d\tau} &= -\frac{3}{4} \sin(2\theta_1), \\ \frac{d\theta_2}{d\tau} &= -\sin(2\theta_2). \end{aligned} \quad (4.43)$$

Label	Coordinates	Eigenvalues	Stability
dS_{++}	$\{\theta_1 = 2n\pi, \theta_2 = 2m\pi\}$	$\{-\frac{3}{2}, -2, 0\}$	stable
dS_{+-}	$\{\theta_1 = 2n\pi, \theta_2 = (2m+1)\pi\}$	$\{-\frac{3}{2}, -2, 0\}$	stable
dS_{-+}	$\{\theta_1 = (2n+1)\pi, \theta_2 = 2m\pi\}$	$\{-\frac{3}{2}, -2, 0\}$	stable
dS_{--}	$\{\theta_1 = (2n+1)\pi, \theta_2 = (2m+1)\pi\}$	$\{-\frac{3}{2}, -2, 0\}$	stable
$R_{+\pm}^{(0)}$	$\{T = 0, \theta_1 = 2n\pi, \theta_2 = \frac{1}{2}(4m \pm 1)\pi\}$	$\{-\frac{3}{2}, 2, \frac{4}{2-\Delta}\}$	saddle
$R_{-\pm}^{(0)}$	$\{T = 0, \theta_1 = (2n+1)\pi, \theta_2 = \frac{1}{2}(4m \pm 1)\pi\}$	$\{-\frac{3}{2}, 2, \frac{4}{2-\Delta}\}$	saddle
$R_{+\pm}^{(1)}$	$\{T = 1, \theta_1 = 2n\pi, \theta_2 = \frac{1}{2}(4m \pm 1)\pi\}$	$\{-\frac{3}{2}, 2, -\frac{4}{2-\Delta}\}$	saddle
$R_{-\pm}^{(1)}$	$\{T = 1, \theta_1 = (2n+1)\pi, \theta_2 = \frac{1}{2}(4m \pm 1)\pi\}$	$\{-\frac{3}{2}, 2, -\frac{4}{2-\Delta}\}$	saddle
$M_{\pm+}^{(0)}$	$\{T = 0, \theta_1 = \frac{1}{2}(4n \pm 1)\pi, \theta_2 = 2m\pi\}$	$\{\frac{3}{2}, -2, \frac{4}{2-\Delta}\}$	saddle
$M_{\pm-}^{(0)}$	$\{T = 0, \theta_1 = \frac{1}{2}(4n \pm 1)\pi, \theta_2 = (2m+1)\pi\}$	$\{\frac{3}{2}, -2, \frac{4}{2-\Delta}\}$	saddle
$M_{\pm+}^{(1)}$	$\{T = 1, \theta_1 = \frac{1}{2}(4n \pm 1)\pi, \theta_2 = 2m\pi\}$	$\{\frac{3}{2}, -2, -\frac{4}{2-\Delta}\}$	saddle
$M_{\pm-}^{(1)}$	$\{T = 1, \theta_1 = \frac{1}{2}(4n \pm 1)\pi, \theta_2 = (2m+1)\pi\}$	$\{\frac{3}{2}, -2, -\frac{4}{2-\Delta}\}$	saddle

Table 3. Equilibrium points/lines of system (4.43).

There exist three classes of equilibrium points/lines: dS , R , and M . The deceleration parameter q evaluated at the lines dS is $q = -1$, thus, it denotes the de Sitter solutions. Evaluating q at the points R and M we have $q = -1 + \frac{4}{(2-\Delta)}$ or $q = -1 + \frac{3}{2-\Delta}$, respectively; i.e. for $\Delta = 0$ they are associated with radiation-dominated and with dust fluid solutions, respectively.

The equilibrium points/lines of system (4.43) are summarized in table 3. The label dS_{++} means that θ_1 and θ_2 are both even multiples of π ; dS_{+-} means that θ_1 is an even multiple of π and θ_2 is an odd multiple of π , and so on. The left sign in kernel R is $+$ if θ_1 is an even multiple of π , and $-$ if it is odd multiple of π . The right sign in kernel R is $+$ if θ_2 is co-terminal of $\frac{\pi}{2}$, and $-$ if it is co-terminal of $-\frac{\pi}{2}$. For kernel M , the left sign is $+$ if θ_1 is co-terminal of $\frac{\pi}{2}$, and $-$ if it is co-terminal of $-\frac{\pi}{2}$, whereas the right sign in kernel M is $+$ if θ_2 is an even multiple of π , and $-$ if it is odd multiple of π . For M , R - points, the upper indexes are (0) or (1) depending on whether $T = 0$ or $T = 1$.

As summarized in table 3, we found three classes of equilibrium points/lines:

1. the family dS , which comprises the lines of equilibrium points dS_{++} , dS_{+-} , dS_{-+} and dS_{--} . They represent the de Sitter solutions and are stable.
2. The family R , which encompass the equilibrium points $R_{+\pm}^{(0)}$, $R_{-\pm}^{(0)}$, $R_{+\pm}^{(1)}$ and $R_{-\pm}^{(1)}$. For $\Delta = 0$, they are associated to radiation-dominated solutions and are saddles.
3. The family M , which contains the equilibrium points $M_{\pm+}^{(0)}$, $M_{\pm-}^{(0)}$, $M_{\pm+}^{(1)}$ and $M_{\pm-}^{(1)}$. For $\Delta = 0$, they are associated with dust fluid solutions and are saddles.

Using $E := \frac{H}{H_0} = \frac{1-T}{T}$ we obtain

$$E' = -E \left[\frac{3 \tan^2(\theta_1) + 4 \tan^2(\theta_2)}{(2-\Delta)(\tan^2(\theta_1) + \sec^2(\theta_2))} \right]. \quad (4.44)$$

This implies that E is a monotonic decreasing function. According to the monotonicity principle, the late time attractors satisfy $T = 1$, whereas the early time attractors satisfy $T = 0$. For a representation of the flow of (4.43), we integrate in the variables T, θ_1, θ_2 and project in a compact set using the ‘‘torus-adapted’’ coordinates

$$\mathbf{T}^1 : \begin{cases} x = \cos \theta_1 (2 + T \cos \theta_2), \\ y = \sin \theta_1 (2 + T \cos \theta_2), \\ z = T \sin \theta_2, \end{cases} \quad (4.45)$$

with $0 \leq T \leq 1, \theta_1, \theta_2 \in [-\pi, \pi]$, with inverse

$$\begin{cases} \theta_1 = \tan^{-1} \left(\frac{y}{x} \right), \\ \theta_2 = \tan^{-1} \left(\frac{z}{\sqrt{x^2 + y^2 - 2}} \right), \\ T = \sqrt{\left(\sqrt{x^2 + y^2 - 2} \right)^2 + z^2}. \end{cases} \quad (4.46)$$

In addition, we present the whole evolution in the space (Ω_m, Ω_r, T) through the transform $(T, \theta_1, \theta_2) \mapsto (\Omega_m, \Omega_r, T)$ where

$$(\Omega_m, \Omega_r) = \left[\left(\frac{2 + \Delta}{2 - \Delta} \right) \frac{1}{\bar{\beta}} - \Omega_{m0} - \Omega_{r0} \right] \frac{T^2}{(1 - T)^2} (\tan^2(\theta_1), \tan^2(\theta_2)). \quad (4.47)$$

The case $T = 1/2$ corresponds to current time. Using these variables we have the system

$$\begin{aligned} \frac{d\Omega_m}{d\tau} &= -\Omega_m \left(\frac{2(1 - T)^2 \bar{\beta} (3\Omega_m + 4\Omega_r)}{(\Delta - 2)\bar{\beta} ((1 - T)^2 \Omega_m - T(T(\Omega_{m0} - \Omega_r + \Omega_{r0}) + 2\Omega_r) + \Omega_r) - (\Delta + 2)T^2} + 3 \right), \\ \frac{d\Omega_r}{d\tau} &= -2\Omega_r \left(\frac{(1 - T)^2 \bar{\beta} (3\Omega_m + 4\Omega_r)}{(\Delta - 2)\bar{\beta} ((1 - T)^2 \Omega_m - T(T(\Omega_{m0} - \Omega_r + \Omega_{r0}) + 2\Omega_r) + \Omega_r) - (\Delta + 2)T^2} + 2 \right), \\ \frac{dT}{d\tau} &= - \frac{(1 - T)^3 T \bar{\beta} (3\Omega_m + 4\Omega_r)}{(\Delta - 2)\bar{\beta} ((1 - T)^2 \Omega_m - T(T(\Omega_{m0} - \Omega_r + \Omega_{r0}) + 2\Omega_r) + \Omega_r) - (\Delta + 2)T^2}. \end{aligned} \quad (4.48)$$

In Figure 6 are represented streamlines of the flow of (4.43) onto the unwrapped solution space (left panel) projected both onto the plane θ_1, θ_2 and the torus \mathbf{T}^1 , setting $T = 1$ (right panel) of the solution space of system (4.43) for the joint constraint value $\Delta = 6.245 \times 10^{-4}$, and the extreme value $\Delta = 1$, respectively.

The results summarized in points 1-3 above are confirmed in Figure 6. That is, the lines of equilibrium points $dS_{++}, dS_{+-}, dS_{-+}$ and dS_{--} (the family dS), denoting the de Sitter solutions, are stable. The equilibrium points $R_{\pm\pm}^{(0)}, R_{\pm\pm}^{(1)}$ and $R_{\pm\pm}^{(1)}$ (the family R), associated to radiation dominated solutions for $\Delta = 0$, are saddles. Finally, the equilibrium points $M_{\pm\pm}^{(0)}, M_{\pm\pm}^{(0)}, M_{\pm\pm}^{(1)}$ and $M_{\pm\pm}^{(1)}$ (the family M), associated to matter dominated solutions for $\Delta = 0$, are saddles.

In Figure 7 streamlines of the flow of (4.48) are presented. We select the values (a) $\Delta = 6.245 \times 10^{-4}, \bar{\beta} = 0.915, \Omega_{m0} = 0.311, \Omega_{r0} = 9 \times 10^{-5}$ obtained from the joint constraints, and (b) $\Delta = 0, \bar{\beta} = 1, \Omega_{m0} = 0.311, \Omega_{r0} = 9 \times 10^{-5}$ for Λ CDM model.

Figure 7 shows, in a phase space, a crucial difference of Barrow Entropy Cosmology (top panel) and Λ CDM (bottom panel) related to the early universe. Barrow Entropy Cosmology does not admits a late-time radiation dominated phase (past attractor) and the solutions

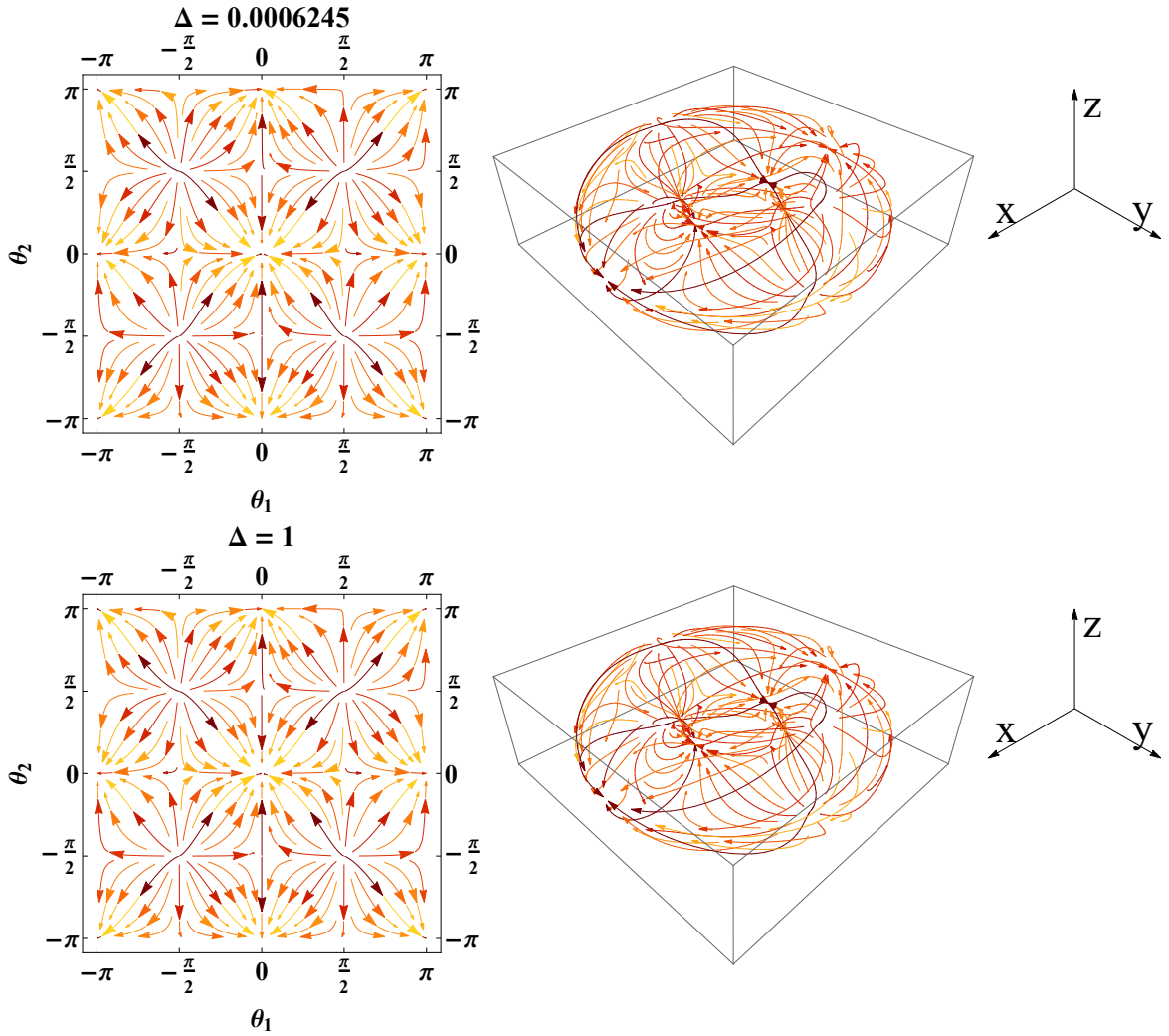


Figure 6. Unwrapped solution space (left panel) projected both onto the plane θ_1, θ_2 and the torus \mathbf{T}^1 given in Cartesian coordinates by (4.45) (right panel) of the solution space of system (4.43) (in the invariant set $T = 1$) for the cases $\Delta = 6.245 \times 10^{-4}$ (top panels), and $\Delta = 1$ (bottom panels).

emerges from the point $(\Omega_r, \Omega_m, T) = (0, 0, 0)$ representing an effective DE- dominated early time attractor. However, both theories have the same late time dynamics, that is, the dominance of a de Sitter phase.

Complementary, we define an unbounded variable \tilde{T} and keep θ_1, θ_2 :

$$\tilde{T} = \frac{H_0}{H}, \quad \theta_1 = \tan^{-1} \left(\sqrt{\frac{8\pi G \rho_m}{\Lambda}} \right), \quad \theta_2 = \tan^{-1} \left(\sqrt{\frac{8\pi G \rho_r}{\Lambda}} \right), \quad (4.49)$$

and using the logarithmic variable $\tau = \ln(a) = -\ln(1+z)$, we obtain the complementary

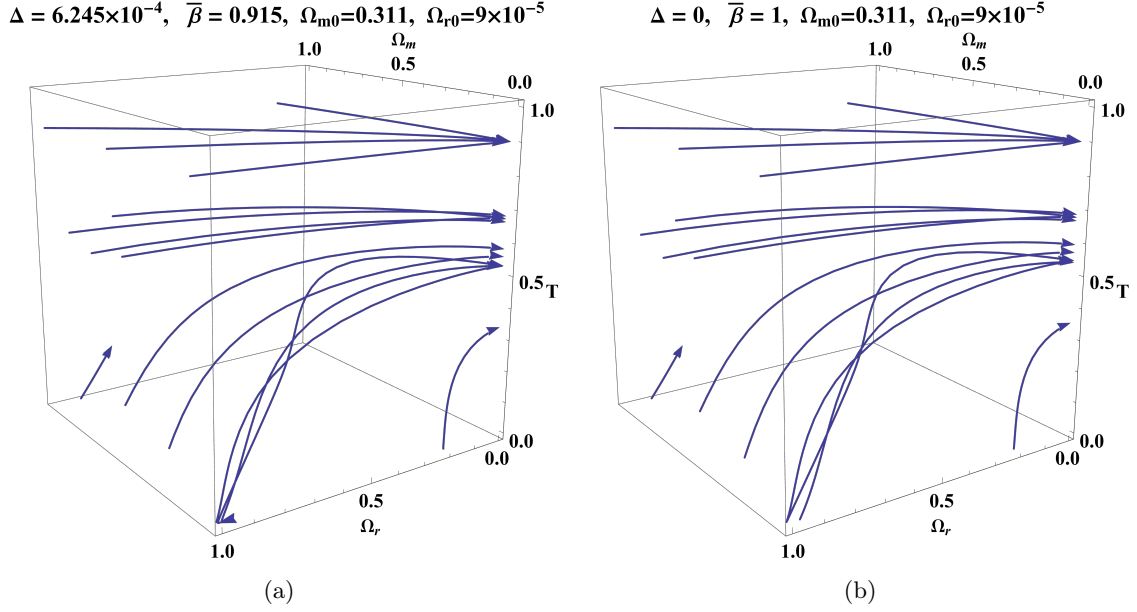


Figure 7. Streamlines of the flow of (4.48) for (a) $\Delta = 6.245 \times 10^{-4}$, $\bar{\beta} = 0.915$, $\Omega_{m0} = 0.311$, $\Omega_{r0} = 9 \times 10^{-5}$ obtained from the joint constraints and (b) $\Delta = 0$, $\bar{\beta} = 1$, $\Omega_{m0} = 0.311$, $\Omega_{r0} = 9 \times 10^{-5}$ for Λ CDM model.

system

$$\begin{aligned}
\frac{d\tilde{T}}{d\tau} &= \frac{\tilde{T} (3 \tan^2(\theta_1) + 4 \tan^2(\theta_2))}{(2 - \Delta) (\tan^2(\theta_1) + \tan^2(\theta_2) + 1)}, \\
\frac{d\theta_1}{d\tau} &= -\frac{3}{4} \sin(2\theta_1), \\
\frac{d\theta_2}{d\tau} &= -\sin(2\theta_2).
\end{aligned} \tag{4.50}$$

Setting $a = 1$ for the current universe, and considering the initial conditions:

$$\theta_1(0) = \tan^{-1} \left(\sqrt{\frac{\Omega_{m0}}{\Omega_{\Lambda 0}}} \right), \quad \theta_2(0) = \tan^{-1} \left(\sqrt{\frac{\Omega_{r0}}{\Omega_{\Lambda 0}}} \right), \quad \tilde{T}(0) = 1, \tag{4.51}$$

the system (4.50) is integrated to obtain

$$\theta_1(\tau) = \tan^{-1} \left(e^{-3\tau/2} \sqrt{\frac{\Omega_{m0}}{\Omega_{\Lambda 0}}} \right), \tag{4.52}$$

$$\theta_2(\tau) = \tan^{-1} \left(e^{-2\tau} \sqrt{\frac{\Omega_{r0}}{\Omega_{\Lambda 0}}} \right), \tag{4.53}$$

$$\tilde{T}(\tau) = e^{-\frac{4\tau}{\Delta-2}} \left(\frac{\Omega_{\Lambda 0} + \Omega_{m0} + \Omega_{r0}}{\Omega_{\Lambda 0}} \right)^{\frac{1}{2-\Delta}} \left(\frac{e^{4\tau} \Omega_{\Lambda 0} + e^{\tau} \Omega_{m0} + \Omega_{r0}}{\Omega_{\Lambda 0}} \right)^{\frac{1}{\Delta-2}}. \tag{4.54}$$

Finally, we work out the exact evolution of H , ρ_m and ρ_r :

$$\begin{aligned} H &= H_0 \left(\frac{\Omega_{\Lambda 0} + e^{-3\tau} \Omega_{m0} + e^{-4\tau} \Omega_{r0}}{\Omega_{\Lambda 0} + \Omega_{m0} + \Omega_{r0}} \right)^{\frac{1}{2-\Delta}} \\ &= H_0 \left(\frac{\Omega_{\Lambda 0} + \Omega_{m0}(1+z)^3 + \Omega_{r0}(1+z)^4}{\Omega_{\Lambda 0} + \Omega_{m0} + \Omega_{r0}} \right)^{\frac{1}{2-\Delta}}, \end{aligned} \quad (4.55)$$

$$\rho_m = \frac{\Lambda \tan^2(\theta_1)}{8\pi G} = \frac{\Lambda e^{-3\tau} \Omega_{m0}}{8\pi G \Omega_{\Lambda 0}} = \frac{3H_0^2 \Omega_{m0}}{8\pi G} (z+1)^3, \quad (4.56)$$

$$\rho_r = \frac{\Lambda \tan^2(\theta_2)}{8\pi G} = \frac{\Lambda e^{-4\tau} \Omega_{r0}}{8\pi G \Omega_{\Lambda 0}} = \frac{3H_0^2 \Omega_{r0}}{8\pi G} (z+1)^4. \quad (4.57)$$

These expressions are used to calculate the fractional energy densities corresponding to matter, radiation, and a Λ -like source as follows:

$$\Omega_m(z) = \frac{8\pi G \rho_m}{3H^2} = \Omega_{m0}(z+1)^3 \left(\frac{\Omega_{\Lambda 0} + \Omega_{m0}(1+z)^3 + \Omega_{r0}(1+z)^4}{\Omega_{\Lambda 0} + \Omega_{m0} + \Omega_{r0}} \right)^{-\frac{2}{2-\Delta}}, \quad (4.58)$$

$$\Omega_r(z) = \frac{8\pi G \rho_r}{3H^2} = \Omega_{r0}(z+1)^4 \left(\frac{\Omega_{\Lambda 0} + \Omega_{m0}(1+z)^3 + \Omega_{r0}(1+z)^4}{\Omega_{\Lambda 0} + \Omega_{m0} + \Omega_{r0}} \right)^{-\frac{2}{2-\Delta}}, \quad (4.59)$$

and

$$\Omega_{\Lambda}(z) = \frac{\Lambda}{3H^2} = \Omega_{\Lambda 0} \left(\frac{\Omega_{\Lambda 0} + \Omega_{m0}(1+z)^3 + \Omega_{r0}(1+z)^4}{\Omega_{\Lambda 0} + \Omega_{m0} + \Omega_{r0}} \right)^{-\frac{2}{2-\Delta}}, \quad \Omega_{\Lambda 0} = \frac{\Lambda}{3H_0^2}. \quad (4.60)$$

From Eq. (2.6) we infer

$$\begin{aligned} \Omega_{DE}(z) &= \frac{8\pi G \rho_{DE}}{3H^2} = \frac{\Lambda}{3H^2} + \left[1 - \frac{\beta(\Delta+2)}{2-\Delta} H^{-\Delta} \right] \\ &= 1 + \Omega_{\Lambda 0} \left(\frac{\Omega_{\Lambda 0} + \Omega_{m0}(1+z)^3 + \Omega_{r0}(1+z)^4}{\Omega_{\Lambda 0} + \Omega_{m0} + \Omega_{r0}} \right)^{-\frac{2}{2-\Delta}} \\ &\quad - \frac{(\Delta+2)}{(2-\Delta)} \frac{1}{\beta} \left(\frac{\Omega_{\Lambda 0} + \Omega_{m0}(1+z)^3 + \Omega_{r0}(1+z)^4}{\Omega_{\Lambda 0} + \Omega_{m0} + \Omega_{r0}} \right)^{-\frac{\Delta}{2-\Delta}} \\ &= 1 + \Omega_{\Lambda 0} \left(\frac{\Omega_{\Lambda 0} + \Omega_{m0}(1+z)^3 + \Omega_{r0}(1+z)^4}{\Omega_{\Lambda 0} + \Omega_{m0} + \Omega_{r0}} \right)^{-\frac{2}{2-\Delta}} \\ &\quad - (\Omega_{\Lambda 0} + \Omega_{m0} + \Omega_{r0}) \left(\frac{\Omega_{\Lambda 0} + \Omega_{m0}(1+z)^3 + \Omega_{r0}(1+z)^4}{\Omega_{\Lambda 0} + \Omega_{m0} + \Omega_{r0}} \right)^{-\frac{\Delta}{2-\Delta}} \\ &= 1 - (\Omega_{m0}(1+z)^3 + \Omega_{r0}(1+z)^4) \left(\frac{\Omega_{\Lambda 0} + \Omega_{m0}(1+z)^3 + \Omega_{r0}(1+z)^4}{\Omega_{\Lambda 0} + \Omega_{m0} + \Omega_{r0}} \right)^{-\frac{2}{2-\Delta}}, \end{aligned} \quad (4.61)$$

where we use Eq. (2.26) to eliminate the term $\left(\frac{2+\Delta}{2-\Delta}\right) \frac{1}{\beta}$, recall $-\frac{\Delta}{2-\Delta} = 1 - \frac{2}{2-\Delta}$, and algebraically manipulate the equations to obtain $\Omega_{DE} = 1 - \Omega_m - \Omega_r$. It is straightforward to obtain Eqs. (4.58), (4.59), (4.60) and (4.61) in terms of the scale factor by replacing $z = (1/a) - 1$. Figure 8 shows the evolution of the density parameters Ω_m , Ω_r and Ω_{DE} vs the scale factor a for two cases: the joint constraints for h , Ω_{m0} , Δ and β shown in Table 1

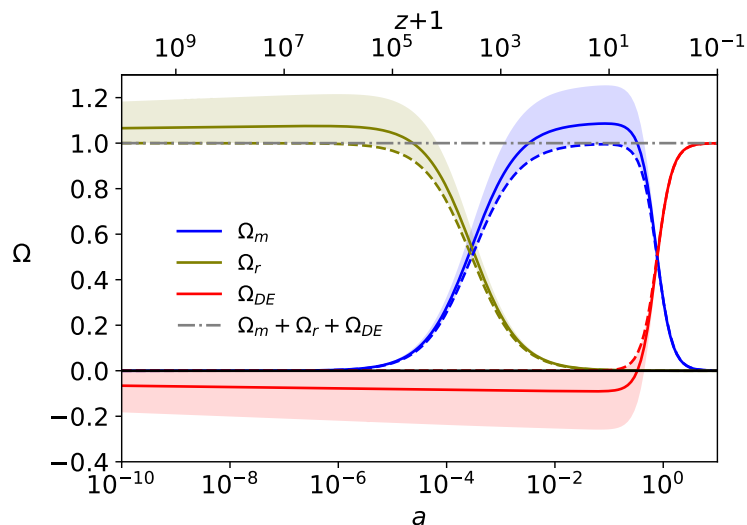


Figure 8. Evolution of the density parameters for matter, radiation, and effective dark energy using the joint constraint of Barrow Cosmology (solid lines) and the values for the standard model $\Delta = 0$, and $\bar{\beta} = 1$ (dashed lines). The shadow regions represent the 3σ confidence levels.

(solid lines), and the values for the standard model $\Delta = 0$, $\bar{\beta} = 1$ (dashed lines). We estimate $\Omega_{r0} \sim 9 \times 10^{-5}$ consistent with the CMB data [2]. The shadowed regions represent the 3σ confidence levels. It is worthy to note that there are values of the energy densities which satisfy $\Omega_m > 1$, $\Omega_r > 1$, and $\Omega_{DE} < 0$, however, these values are close to Λ CDM lines within the 3σ error propagation.

5 Summary and discussion

Barrow entropy cosmology is a recent model [20] based on the modification of the entropy-area black hole relation proposed by Barrow [19] that involves a new parameter Δ , recovering the standard form of the Bekenstein entropy for $\Delta = 0$. Considering this new relation, the modified Friedmann equations governing the dynamics of the Universe can be obtained from the gravity-thermodynamics approach. These new equations contain two parameters Δ , and $\bar{\beta}$ (where the standard model is recovered for $\Delta = 0$ and $\bar{\beta} = 1$) and could source the cosmic acceleration at late times. We investigate two Barrow cosmological models: I) Universe filled only by a matter component and II) Universe filled by matter and radiation components. Furthermore, we divide the study of Barrow proposition in two ways: an observational approach and a dynamical system stability analysis.

For the first approach we constrained the free parameters Δ , h , and Ω_{m0} , for both cosmological models, employing the observational Hubble data, type Ia supernovae, HII galaxies, strong lensing systems, baryon acoustic oscillations, and a joint analysis of these samples. We provide the observational constraints in section 3 (see table 1), showing that for the model I the Barrow parameters are $\Delta = (5.912^{+3.353}_{-3.112}) \times 10^{-4}$, $\bar{\beta} = 0.920^{+0.042}_{-0.042}$, and for the model II $\Delta = (6.245^{+3.377}_{-3.164}) \times 10^{-4}$, $\bar{\beta} = 0.915^{+0.043}_{-0.043}$. For both models these constraints are consistent at 2σ with both the standard cosmological model and the standard entropy-area entropy relation. By reconstructing the cosmic expansion rate using the joint constraints in both cosmologies, we found consistency with the observational Hubble data. In addition, for the more realistic

model with matter and radiation components, we calculated the deceleration parameter and obtained a transition at $z_t \simeq 0.711_{-0.034}^{+0.035}$ from a decelerated stage to an accelerated stage with $q_0 = -0.573_{-0.019}^{+0.019}$, suggesting a de Sitter solution. We also confirm that, under these cosmologies, the equation of state of the effective dark energy can undergo from a quintessence-like regime to a phantom-like one as found by [20], yielding $w_{DE}(0) \simeq -1.000134_{-0.000068}^{+0.000069}$ at current times which is consistent with the cosmological constant at 1σ . Furthermore, we estimated the age of the Universe as $t_0 \simeq 14.062_{-0.170}^{+0.179}$ Gyr, consistent within 2σ confidence level with the measurements of Planck [2].

The second approach, the stability analysis, allowed to find regions on the parameter space where the different cosmic epochs take place. In this regard, we obtained a qualitative description of the local and global dynamics of both cosmological scenarios, irrespective of the initial conditions and the specific evolution of the universe. Moreover, we have found asymptotic solutions calculated various theoretical values for the observable quantities that can be compared with previous observational constraints. From the analysis at the finite region of the phase space in the model I, we have found the line $A(\Omega_\Lambda)$ of equilibrium points, which is the attractor of the system and represents the de Sitter solutions. For $\Delta = 0$, the line $B(\Omega_m)$ contains the past attractors, which represents the matter dominated solutions. Additionally, we have defined the compact variables (assuming $H \geq 0, H_0 > 0$) based on the approach by [56]. We have found two equivalent (due to the discrete symmetry) hyperbolic fixed points M_\pm associated with dust fluid for $\Delta = 0$, and two equivalent fixed points dS_\pm corresponding to the de Sitter states (see Table 2). On the other hand, in the model II, the line $A(\Omega_\Lambda)$ is the attractor of the system and represents the de Sitter solutions. For $\Delta = 0$, the line $B(\Omega_m)$ is a saddle, indicating the matter dominated solutions, while the line $C(\Omega_r)$ contains the past attractors and specify the radiation dominated solutions. Finally, we found three classes of equilibrium points/ lines: dS , R and M ; with dS denoting the de Sitter solutions, and for $\Delta = 0$, R and M are the radiation-dominated and dust fluid solutions, respectively (see Table 3).

For both models we reconstruct the evolution of the density parameters Ω_m , Ω_r , and Ω_{DE} as a function of the scale factor a for two cases: using the joint constraints for h , Ω_{m0} , Δ and $\bar{\beta}$, and the values for the standard model $\Delta = 0$, $\bar{\beta} = 1$ (see Figs. 5 and 8). We found that at the early times there are values of the energy densities which satisfy $\Omega_m > 1$, $\Omega_r > 1$, and $\Omega_{DE} < 0$. However, these values are close to Λ CDM lines within the 3σ error propagation. Thus, with more and high precision cosmological data, these non-physical density parameter values could be avoided.

A crucial difference of Barrow Entropy Cosmology and the standard Λ CDM model is related to the early universe. Barrow Entropy Cosmology does not admits a late-time radiation dominated phase and the solutions are past asymptotic to a point representing an effective DE- dominated early time attractor. However, both theories have the same late time dynamics, that is, the dominance of a de Sitter phase. In summary, we have showed, from several points of view, that the dynamical equations have a de Sitter solution at late times but the dynamics at early times is not consistent with the evolution of the standard cosmological model.

Acknowledgments

The authors are grateful for the figure 7 provided by Alfredo D. Millano (PhD student at Universidad Católica del Norte (UCN)). G.L. was funded by Agencia Nacional de Investigación

y Desarrollo - ANID for financial support through the program FONDECYT Iniciación grant no. 11180126 and by Vicerrectoría de Investigación y Desarrollo Tecnológico at UCN. J.M. acknowledges the support from ANID project Basal AFB-170002 and ANID REDES 190147. M.A.G.-A. acknowledges support from SNI-México, CONACyT research fellow, ANID REDES (190147), COZCyT and Instituto Avanzado de Cosmología (IAC). A.H.A. thanks to the PRODEP project, Mexico for resources and financial support and thanks also to the support from Luis Aguilar, Alejandro de León, Carlos Flores, and Jair García of the Laboratorio Nacional de Visualización Científica Avanzada. V.M. acknowledges support from Centro de Astrofísica de Valparaíso and ANID REDES 190147.

References

- [1] A.G. Riess, A.V. Filippenko, P. Challis, A. Clocchiatti, A. Diercks et al., Observational evidence from supernovae for an accelerating universe and a cosmological constant, The Astronomical Journal **116** (1998) 1009.
- [2] PLANCK collaboration, Planck 2018 results. VI. Cosmological parameters, [1807.06209](#).
- [3] S. Nadathur, W.J. Percival, F. Beutler and H. Winther, Testing Low-Redshift Cosmic Acceleration with Large-Scale Structure, Phys. Rev. Lett. **124** (2020) 221301 [[2001.11044](#)].
- [4] S.M. Carroll, The Cosmological constant, Living Rev. Rel. **4** (2001) 1 [[astro-ph/0004075](#)].
- [5] D. Lovelock, The einstein tensor and its generalizations, Journal of Mathematical Physics **12** (1971) 498 [<https://doi.org/10.1063/1.1665613>].
- [6] S. Weinberg, The cosmological constant problem, Rev. Mod. Phys. **61** (1989) 1.
- [7] Y. Zel'dovich, A. Krasinski and Y. Zeldovich, The Cosmological constant and the theory of elementary particles, Sov. Phys. Usp. **11** (1968) 381.
- [8] M.A. García-Aspeitia, J. Magaña, A. Hernández-Almada and V. Motta, Probing dark energy with braneworld cosmology in the light of recent cosmological data, Int. J. Mod. Phys. D **27** (2018) 18560006 [[1609.08220](#)].
- [9] M.A. García-Aspeitia, A. Hernández-Almada, J. Magaña, M.H. Amante, V. Motta and C. Martínez-Robles, Brane with variable tension as a possible solution to the problem of the late cosmic acceleration, Phys. Rev. D **97** (2018) 101301 [[1804.05085](#)].
- [10] M.A. García-Aspeitia, C. Martínez-Robles, A. Hernández-Almada, J. Magaña and V. Motta, Cosmic acceleration in unimodular gravity, Phys. Rev. D **99** (2019) 123525 [[1903.06344](#)].
- [11] M.A. García-Aspeitia, A. Hernández-Almada, J. Magaña and V. Motta, The Universe acceleration from the Unimodular gravity view point: Background and linear perturbations, Phys. Dark Univ. **32** (2021) 100840 [[1912.07500](#)].
- [12] V. Motta, M.A. García-Aspeitia, A. Hernández-Almada, J. Magaña and T. Verdugo, Taxonomy of dark energy models, Universe **7** (2021) .
- [13] Hernández-Almada, A., Magaña, Juan, García-Aspeitia, Miguel A. and Motta, V., Cosmological constraints on alternative model to chaplygin fluid revisited, Eur. Phys. J. C **79** (2019) 12.
- [14] A. Hernández-Almada, M.A. García-Aspeitia, J. Magaña and V. Motta, Stability analysis and constraints on interacting viscous cosmology, Phys. Rev. D **101** (2020) 063516 [[2001.08667](#)].

- [15] A. Hernández-Almada, G. Leon, J. Magaña, M.A. García-Aspeitia and V. Motta, Generalized Emergent Dark Energy: observational Hubble data constraints and stability analysis, [Mon. Not. Roy. Astron. Soc.](#) **497** (2020) 1590 [2002.12881].
- [16] J.D. Bekenstein, Black holes and entropy, [Phys. Rev. D](#) **7** (1973) 2333.
- [17] T. Jacobson, Thermodynamics of space-time: The Einstein equation of state, [Phys. Rev. Lett.](#) **75** (1995) 1260 [gr-qc/9504004].
- [18] R.-G. Cai and S.P. Kim, First law of thermodynamics and Friedmann equations of Friedmann-Robertson-Walker universe, [JHEP](#) **02** (2005) 050 [hep-th/0501055].
- [19] J.D. Barrow, The Area of a Rough Black Hole, [Phys. Lett. B](#) **808** (2020) 135643 [2004.09444].
- [20] E.N. Saridakis, Modified cosmology through spacetime thermodynamics and Barrow horizon entropy, [JCAP](#) **07** (2020) 031 [2006.01105].
- [21] E.N. Saridakis, Barrow holographic dark energy, [Phys. Rev. D](#) **102** (2020) 123525 [2005.04115].
- [22] F.K. Anagnostopoulos, S. Basilakos and E.N. Saridakis, Observational constraints on Barrow holographic dark energy, [2005.10302](#).
- [23] A.A. Mamon, A. Paliathanasis and S. Saha, Dynamics of an Interacting Barrow Holographic Dark Energy Model and its Thermodynamic Implications, [Eur. Phys. J. Plus](#) **136** (2021) 134 [2007.16020].
- [24] P. Adhikary, S. Das, S. Basilakos and E.N. Saridakis, Barrow Holographic Dark Energy in non-flat Universe, [2104.13118](#).
- [25] E.N. Saridakis and S. Basilakos, The generalized second law of thermodynamics with Barrow entropy, [2005.08258](#).
- [26] E. Komatsu and et. al. [The Astrophysical Journal Supplement Series](#) **192** (2011) 18.
- [27] J. Magaña, M.H. Amante, M.A. García-Aspeitia and V. Motta, The Cardassian expansion revisited: constraints from updated Hubble parameter measurements and type Ia supernovae, [Mon. Not. Roy. Astron. Soc.](#) **476** (2018) 1036 [1706.09848].
- [28] D.M. Scolnic et al., The Complete Light-curve Sample of Spectroscopically Confirmed SNe Ia from Pan-STARRS1 and Cosmological Parameters, [Astrophys. J.](#) **859** (2018) 101 [1710.00845].
- [29] S. Cao, J. Ryan and B. Ratra, Cosmological constraints from HII starburst galaxy apparent magnitude and other cosmological measurements, [Mon. Not. Roy. Astron. Soc.](#) **497** (2020) 3191 [2005.12617].
- [30] M.H. Amante, J. Magaña, V. Motta, M.A. García-Aspeitia and T. Verdugo, Testing dark energy models with a new sample of strong-lensing systems, [1906.04107](#).
- [31] R.C. Nunes, S.K. Yadav, J. Jesus and A. Bernui, Cosmological parameter analyses using transversal BAO data, [Mon. Not. Roy. Astron. Soc.](#) **497** (2020) 2133 [2002.09293].
- [32] M. Moresco, L. Pozzetti, A. Cimatti, R. Jimenez, C. Maraston, L. Verde et al., A 6% measurement of the Hubble parameter at $z \sim 0.45$: direct evidence of the epoch of cosmic re-acceleration, [JCAP](#) **1605** (2016) 014 [1601.01701].
- [33] D.M. Scolnic et al., The Complete Light-curve Sample of Spectroscopically Confirmed SNe Ia from Pan-STARRS1 and Cosmological Parameters, [Astrophys. J.](#) **859** (2018) 101 [1710.00845].

- [34] R. Chávez, E. Terlevich, R. Terlevich, M. Plionis, F. Bresolin, S. Basilakos et al., Determining the Hubble constant using giant extragalactic H II regions and H II galaxies, [*Mon. Not. R. Ast. Soc.* **425** \(2012\) L56 \[1203.6222\]](#).
- [35] R. Chávez, R. Terlevich, E. Terlevich, F. Bresolin, J. Melnick, M. Plionis et al., The L- σ relation for massive bursts of star formation, [*Mon. Not. R. Ast. Soc.* **442** \(2014\) 3565 \[1405.4010\]](#).
- [36] R. Terlevich, E. Terlevich, J. Melnick, R. Chávez, M. Plionis, F. Bresolin et al., On the road to precision cosmology with high-redshift H II galaxies, [*Mon. Not. R. Ast. Soc.* **451** \(2015\) 3001 \[1505.04376\]](#).
- [37] R. Chávez, M. Plionis, S. Basilakos, R. Terlevich, E. Terlevich, J. Melnick et al., Constraining the dark energy equation of state with H II galaxies, [*Mon. Not. R. Ast. Soc.* **462** \(2016\) 2431 \[1607.06458\]](#).
- [38] A.L. González-Morán, R. Chávez, R. Terlevich, E. Terlevich, F. Bresolin, D. Fernández-Arenas et al., Independent cosmological constraints from high-z H II galaxies, [*Mon. Not. R. Ast. Soc.* **487** \(2019\) 4669 \[1906.02195\]](#).
- [39] A.L. González-Morán, R. Chávez, E. Terlevich, R. Terlevich, D. Fernández-Arenas, F. Bresolin et al., Independent cosmological constraints from high-z H II galaxies: new results from VLT-KMOS data, [*Mon. Not. Roy. Astron. Soc.* **505** \(2021\) 1441 \[2105.04025\]](#).
- [40] R. Giostri, M.V. dos Santos, I. Waga, R. Reis, M. Calvão and B.L. Lago, From cosmic deceleration to acceleration: new constraints from SN Ia and BAO/CMB, [*Journal of Cosmology and Astroparticle Physics* **2012** \(2012\) 027](#).
- [41] W.J. Percival, B.A. Reid, D.J. Eisenstein, N.A. Bahcall, T. Budavari, J.A. Frieman et al., Baryon acoustic oscillations in the Sloan Digital Sky Survey Data Release 7 galaxy sample, [*Monthly Notices of the Royal Astronomical Society* **401** \(2010\) 2148 \[https://academic.oup.com/mnras/article-pdf/401/4/2148/3901461/mnras0401-2148.pdf\]](#).
- [42] C. Blake, E.A. Kazin, F. Beutler, T.M. Davis, D. Parkinson, S. Brough et al., The WiggleZ Dark Energy Survey: mapping the distance-redshift relation with baryon acoustic oscillations, [*Monthly Notices of the Royal Astronomical Society* **418** \(2011\) 1707 \[https://academic.oup.com/mnras/article-pdf/418/3/1707/18440857/mnras0418-1707.pdf\]](#).
- [43] F. Beutler, C. Blake, M. Colless, D.H. Jones, L. Staveley-Smith, L. Campbell et al., The 6dF Galaxy Survey: baryon acoustic oscillations and the local Hubble constant, [*mnras* **416** \(2011\) 3017 \[1106.3366\]](#).
- [44] SDSS collaboration, Detection of the baryon acoustic peak in the large-scale correlation function of SDSS luminous red galaxies, [*Astrophys. J.* **633** \(2005\) 560](#).
- [45] D. Foreman-Mackey, D.W. Hogg, D. Lang and J. Goodman, [*emcee: The MCMC Hammer*](#), [*pasp* **125** \(2013\) 306 \[1202.3665\]](#).
- [46] J. Wainwright and G.F.R. Ellis, [*Dynamical Systems in Cosmology*](#), Cambridge University Press (1997).
- [47] P.G. Ferreira and M. Joyce, Structure formation with a selftuning scalar field, [*Phys. Rev. Lett.* **79** \(1997\) 4740 \[astro-ph/9707286\]](#).
- [48] E.J. Copeland, A.R. Liddle and D. Wands, Exponential potentials and cosmological scaling solutions, [*Phys. Rev.* **D57** \(1998\) 4686 \[gr-qc/9711068\]](#).
- [49] L. Perko, [*Differential Equations and Dynamical Systems, Third Edition*](#), Springer (2000).

- [50] A.A. Coley, *Dynamical systems and cosmology*, vol. 291, Kluwer, Dordrecht, Netherlands (2003), [10.1007/978-94-017-0327-7](https://doi.org/10.1007/978-94-017-0327-7).
- [51] E.J. Copeland, M. Sami and S. Tsujikawa, *Dynamics of dark energy*, [*Int. J. Mod. Phys. D* **15** \(2006\) 1753](#) [[hep-th/0603057](#)].
- [52] X.-m. Chen, Y.-g. Gong and E.N. Saridakis, *Phase-space analysis of interacting phantom cosmology*, [*JCAP* **0904** \(2009\) 001](#) [[0812.1117](#)].
- [53] S. Cotsakis and G. Kittou, *Flat limits of curved interacting cosmic fluids*, [*Phys. Rev. D* **88** \(2013\) 083514](#) [[1307.0377](#)].
- [54] R. Giambo and J. Miritzis, *Energy exchange for homogeneous and isotropic universes with a scalar field coupled to matter*, [*Class. Quant. Grav.* **27** \(2010\) 095003](#) [[0908.3452](#)].
- [55] B. Aulbach, *Continuous and Discrete Dynamics Near Manifolds of Equilibria*, *Lecture Notes in Mathematics*, Springer (1984).
- [56] A. Alho and C. Ugglá, *Global dynamics and inflationary center manifold and slow-roll approximants*, [*J. Math. Phys.* **56** \(2015\) 012502](#) [[1406.0438](#)].